Developmental fine-tuning of
excitatory synaptic transmission at input synapses
in the rat inferior colliculus

DOCTORAL DISSERTATION

By:

Mako Kitagawa

Graduate School of Brain Science, Doshisha University

Supervisor:

Dr. Takeshi Sakaba

A thesis submitted for the degree of

Doctor of Philosophy in Science

March 2020

Abstract

The inferior colliculus (IC) is the primal center of convergence and integration in the auditory pathway. Although extensive functional changes are known to occur at the relay synapses in the auditory brainstem during development, the changes in the IC remain to be investigated. Here, I have measured excitatory synaptic currents (EPSCs) of the neurons in the central nucleus of the IC in response to stimulation of the lateral lemniscus and the commissure of the inferior colliculus. Before hearing onset, the lemniscus inputs exhibited short-term depression, whereas commissural inputs showed facilitation. After hearing onset, the NMDA-EPSCs exhibited faster decay for both pathways, whereas the decay of the AMPA-EPSCs were unaltered. Furthermore, the EPSCs showed more constant responses during repetitive stimulation in both pathways. These developmental changes may ensure faster and more reliable signal transmission to the inferior colliculus after onset of hearing.

Acknowledgements

Table of contents

List of tables

List of figures

1. Introduction

1.1. Background

The localization of sound is performed by the auditory nervous system. To locate a sound source, auditory information from each ear is processed separately, by the cochlear nucleus (CN), and is converged at the superior olivary complex (SOC) in the auditory brainstem. Afferent projections from these nuclei converge in the inferior colliculus (IC). IC neurons are considered to compute sound location. Moreover, commissural connections between the contralateral and ipsilateral IC enhances the response of IC neurons (Orton *et al.*, 2016) and may play a role in sound localization.

In sensory systems, neural activity adjusts synaptic and circuit functions by sensory experience during development. In the auditory pathway of rodents, morphological and functional properties change dramatically during postnatal development, especially around the onset of sensory inputs. For example, the first two weeks of postnatal development transforms synapse operation from moderate to very high-frequency signaling, allowing for high-fidelity signal transmission (Schneggenburger & Forsythe, 2006). However, how synaptic response properties in the central nucleus of the inferior colliculus (CNIC) change around the onset of hearing remains uncertain. This study mainly focuses on how these changes occur.

I will first provide some general information about the IC in the auditory pathway and synaptic maturation in the IC.

1.2. An overview of the ascending auditory pathway.

Auditory neurons encode and extract various properties of sound. Sound coming from the external ear induces vibrations of the tympanic membrane. Hair cells in the cochlea detect these vibrations and release the neurotransmitter glutamate in response to transmit the signals to the CN (Winer & Schreiner, 2005; Brian, 2013). The auditory information passes many nuclei from the CN to the cerebral cortex. The central auditory pathway is composed of an interconnected network of relay stations such as the CN, the SOC, the lateral lemniscus, the IC, the medial geniculate body, and the auditory cortex (Fig. 1). Before reaching the cerebral cortex, auditory information is processed within a particular nucleus or by interaction between multiple nuclei by feedforward and feedback pathways.
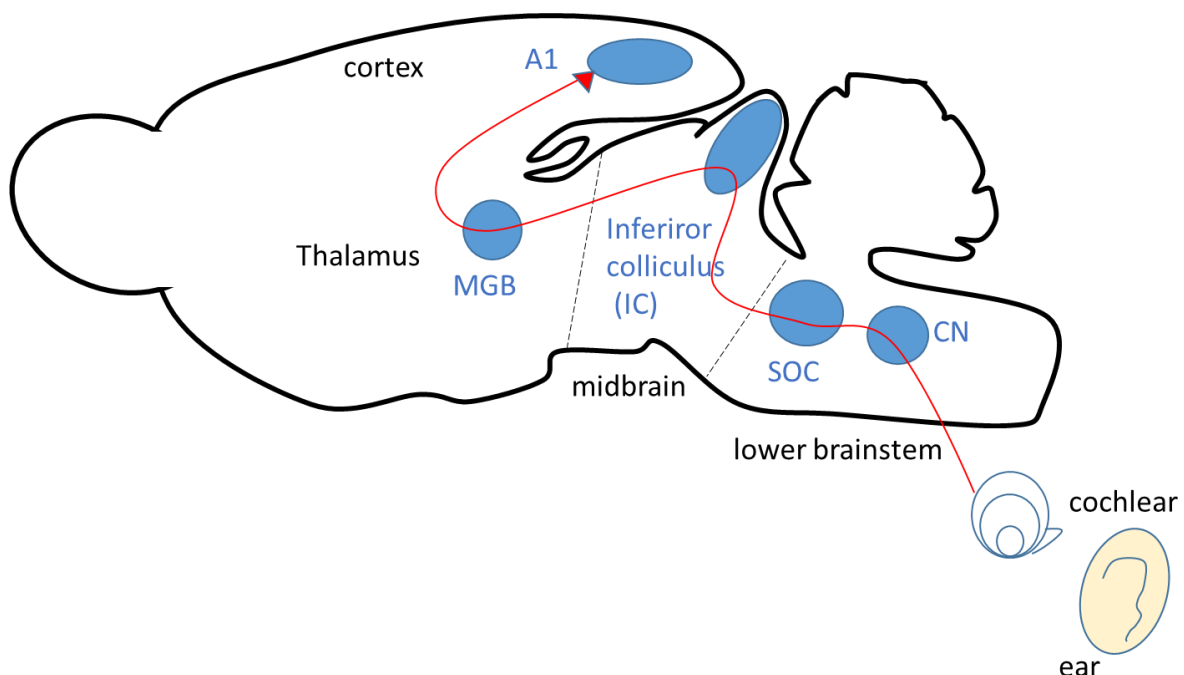
Figure 1. Schematic drawing of ascending auditory pathway in the rats.
The auditory information is transmitted from the cochlear nucleus (CN) to the primary auditory cortex (A1) by passing through many relay stations, such as superior olivary complex (SOC), lateral lemniscus, inferior colliculus (IC), medial geniculate body (MGB), and auditory cortex. See Winer & Schreiner (2005), Caspary *et al.* (2008), and Asaba *et al.*, (2014) for details.

When sound information is transmitted from the cochlea to the CN and is segregated into different brainstem regions, different aspects of sounds such as sound intensity and the timing of sound onsets, are encoded. The majority of ascending signals from the brainstem regions are integrated at the IC in the midbrain. Neurons of the IC sending outputs to the thalamus display selective responses to various physical features of sounds. For example, the spectral, temporal, and binaural disparities of sounds are encoded by different neurons (Ehret & Schreiner, 2005). The spatial location of sound source information is computed by the binaural disparity of sounds. Within the barn owl IC, spatial location cues of sound source information are synthesized from horizontal and vertical cues measured by both ears (Knudsen, 2002).

1.3. General overview of the IC in the auditory pathway and synaptic inputs
1.3.1. Afferent synapses to the IC in the auditory midbrain pathway

The IC is the primary subcortical auditory center of convergence and integration in the mammalian midbrain. The main subdivision of the mammalian IC is the central nucleus. A main feature of the CNIC is the fibrodendritic lamina, an entity comprising disc-shaped neurons in which the laminar plexus of afferent axons terminate (Oliver, 2005). In the CNIC, axons from the lower auditory brainstem ascend through the lateral lemniscus (LL) and synapse onto CNIC neurons (Cant, 2013; Ono & Ito, 2015). Other major inputs, referred to as commissural inputs, pass through the commissure of the inferior colliculus (CoIC) from the contralateral IC to the CNIC (Saldaña & Merchań, 1992; Malmierca *et al.*, 2009). Intracellular studies in gerbil coronal brain slices have shown that most CNIC neurons receive convergent inputs from the LL and the contralateral IC via commissural projections (Moore *et al.*, 1998).

1.3.2. The CNIC neurons receive ascending synaptic inputs in the auditory pathway

CNIC neurons receive ascending excitatory inputs from the medial superior olive (MSO), the lateral superior olive (LSO), the dorsal cochlear nucleus (DCN), and the ventral cochlear nucleus (Kelly & Caspary, 2005). Simultaneously, CNIC neurons receive ascending inhibitory inputs from the LSO, the ventral nucleus of the lateral lemniscus, and the dorsal nucleus of the lateral lemniscus (DNLL) (Kelly & Caspary, 2005). The largest afferent source of each IC is the contralateral IC (Moore *et al.*, 1998). CoIC fibers are both glutamatergic and GABAergic (Nakamoto *et al.*, 2013; Ito & Oliver, 2014).
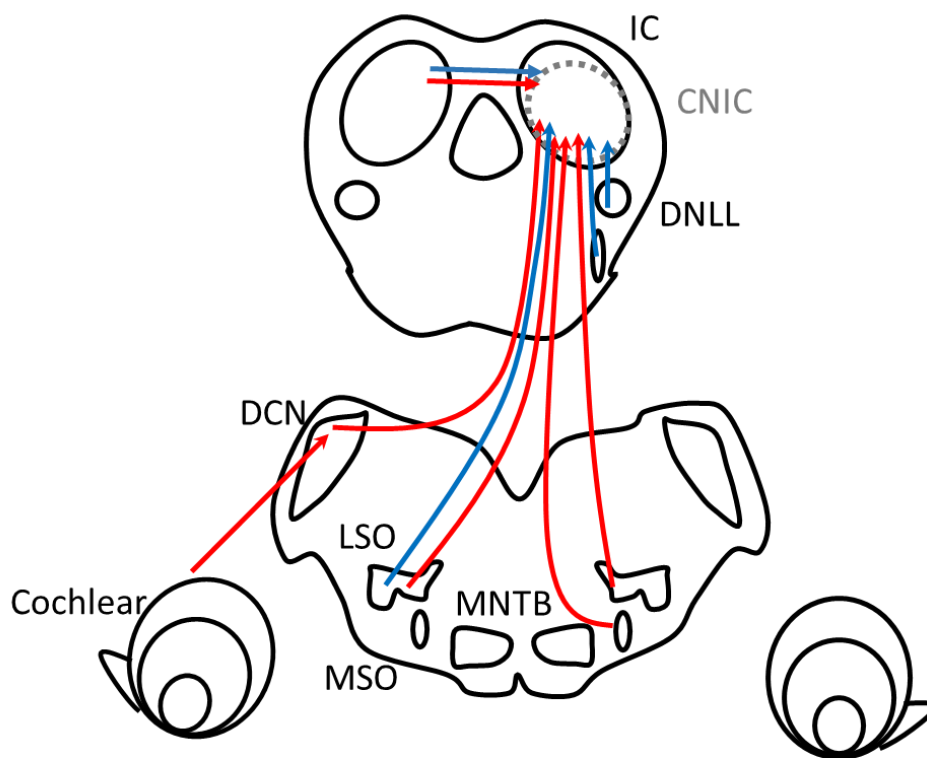
Figure 2. Schematic drawings of ascending auditory pathways of the mammalian midbrain inferior colliculus. Red lines indicate excitatory pathways. Blue lines indicate inhibitory pathways, respectively. See Winer & Schreiner (2005), Caspary *et al.* (2008), Ono & Oliver (2014), and Ono & Ito (2015) for details.

A recent study in mice showed that excitatory CNIC neurons receive excitatory inputs from different combinations of specific nuclei. Inhibitory neurons, in contrast, receive inputs from the same combination of all nuclei (Chen et al., 2018).

Ipsilateral and contralateral LSOs send extensive excitatory inputs to the CNIC (Oliver, 2005). The inputs from ipsilateral and contralateral LSOs and those from the MSO overlap in the CNIC, and these inputs are distributed heterogeneously within the CNIC (Cant, 2013). In addition to excitatory inputs, the ipsilateral LSO also provides inhibitory inputs to the CNIC. DNLL provides inputs to the dorsolateral CNIC (Cant & Benson, 2006). Principal cells in the medial nucleus of the trapezoid body do not send inputs to the IC, but lateral nucleus of the trapezoid body (LNTB) innervates bilaterally to the IC (Cant, 2013)

Ipsilateral and contralateral CN innervates lateral part of the CNIC. The inputs from the CN are distributed heterogeneously within the CNIC. Patch-like innervation patterns from the ipsilateral and contralateral CN do not overlap fully within CNIC (Cant & Benson, 2008). Oliver and colleagues found that the ipsilateral anteroventral CN constitutes up to 18 % of the excitatory terminals in the pars lateralis CNIC, whereas the contralateral anteroventral CN constitutes up to 13 %. The contralateral DCN constitutes up to 11 % of the excitatory terminals (Oliver, 2005; Cant, 2013).

Previous studies have demonstrated that commissural neurons in the CNIC send divergent projections to the equivalent frequency-band laminae in the CNIC and the dorsal and lateral cortices on the opposite side (Malmierca *et al.*, 2005). In a more recent study, the superior paraolivary nucleus, which mainly projects GABAergic axons to the ipsilateral IC, was shown to also send GABAergic axons to the contralateral IC via the CoIC (Saldaña *et al.*, 2009).

1.4. The morphology and physiological cell types of the IC

IC neurons show diverse responses to sounds and differ morphologically and physiologically.

1.4.1. Physiological heterogeneity of IC neurons

. *In vivo* extracellular recordings showed that IC neurons respond to specific sound frequencies and are arranged tonotopically (Palmer *et al.*, 2013). In addition, there are different types of firing patterns in response to sounds. Firing of the IC neurons do not necessarily follow sound stimulation, as seen in the lower auditory brainstem. For example, some IC neurons show stimulus-specific adaptation to sounds and reduce their responses when stimulated repetitively (Pérez-González & Malmierca, 2014). *In vivo* whole-cell recordings showed that GABAergic and glutamatergic IC neurons exhibit similar responses to pure tones but their ability to follow amplitude modulation is different (Ono *et al.*, 2017). The offset neurons are known as the neurons firing at the sound stimuli offset and are induced by several underlying cellular and circuit mechanisms, (Kasai *et al.*, 2012).

The mechanisms underlying the heterogeneous response properties remain to be elucidated. *In vitro* whole-cell recordings in IC neurons revealed heterogeneous intrinsic firing patterns. Six firing patterns were found in response to depolarizing and hyperpolarizing current pulses (Sivaramakrishnan & Oliver, 2001). These diverse firing patterns do not directly correlate to the neuronal morphology or neurotransmitter phenotype (Reetz & Ehret, 1999; Peruzzi *et al.*, 2000; Sivaramakrishnan & Oliver, 2001; Ono *et al.*, 2005).

1.4.2. Morphological heterogeneity of IC neurons

The majority of CNIC neurons are classified into two main types by studies using three-dimensional reconstructions of Golgi impregnated neurons in rats: flat neurons and less flat neurons.

Flat neurons have flattened dendritic arbors. Less-flat neurons have less flat dendritic trees and their dendritic arbors often extend across the laminae (Oliver, 2005). The thickness of the dendritic arbor in flat neurons is 50–70 µm. Less-flat neurons cross the axis of the fibrodendritic laminae, although the dendritic trees are thicker (approx. 100 µm) and less dense compared to those of flat neurons (Ito & Malmierca, 2018).

1.5. Synaptic transmission and short-term plasticity

1.5.1 Synaptic transmission at chemical synapses

Chemical synapses transmit signals from presynaptic to postsynaptic cells (Fig. 3). Chemical transmission is composed of two processes. The first process is the release of neurotransmitters. When an action potential reaches the presynaptic axon terminal, it elicits Ca^{2+} influx through voltage-gated Ca^{2+} channels in the terminal. Ca^{2+} influx triggers the fusion of neurotransmitter-containing synaptic vesicles with the plasma membrane and the release of neurotransmitters into the extracellular space, called the synaptic cleft. The second process is the binding of the released transmitter to receptors and activating them. The postsynaptic responses depend on the type of receptor. For example, glutamate can activate ionotropic glutamate receptors, such as α-amino-3-5-methyl-4-isoxazolepropionic acid (AMPA) receptors and N-methyl-D-aspartate (NMDA) receptors (Fig. 3) AMPA receptors, permeable to Na^+ and K^+, activate and deactivate rapidly within milliseconds, desensitize upon prolonged application of glutamate, and mediate rapid signal transmission between neurons. NMDA receptors activate and deactivate more slowly within tens of milliseconds, desensitize to a lesser degree, and are also important for induction of long-term synaptic plasticity

through permeation of Ca^{2+} into postsynaptic neurons. Furthermore, G-protein-coupled metabotropic glutamate receptors (mGluRs) are coupled to second messengers, exerting excitatory or inhibitory action on a much slower time scale (Kandel *et al.*, 2000). Similarly, GABA receptors are classified into several types. $GABA_A$ receptors are ionotropic receptors and permeate Cl^- whereas $GABA_B$ receptors are metabotropic receptors. Glycine receptors are considered to be ionotropic. The ionotropic glutamate receptor (iGluR) family has structurally related glutamate-gated excitatory channels that differ in their sensitivities and responses. NMDA, AMPA, and kainate receptors belong to the iGluR family (Iacobucci & Popescu, 2017).
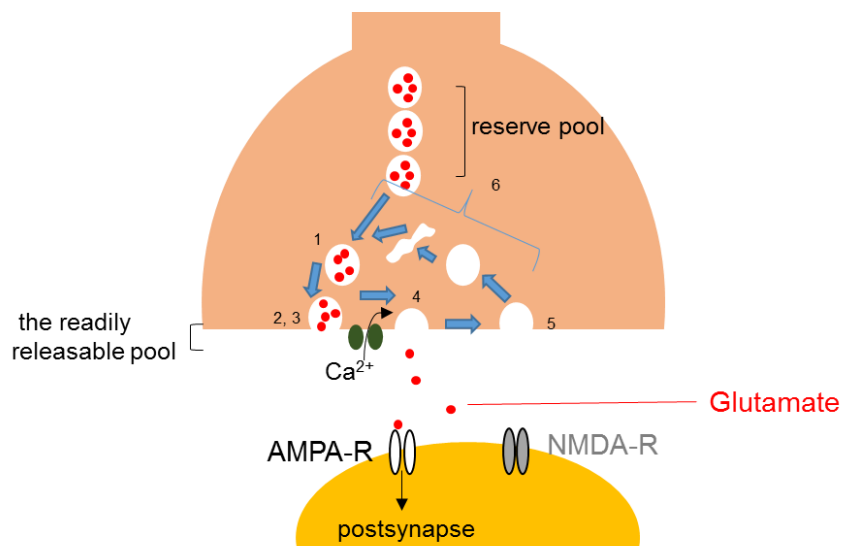
Figure 3. Basic mechanisms of synaptic transmission
Invasion of presynaptic action potentials to the presynaptic terminal opens Ca channels, and Ca influx into the terminal triggers release of neurotransmitters that act on postsynaptic receptors and modulate postsynaptic activity. Excitatory synapses enhance firing of the postsynaptic neurons and inhibitory synapses do the opposite, or cause shunting inhibition, blocking the excitatory action of other inputs. Excitatory neurotransmitter, glutamate can activate ionotoropic glutamate receptors, such as fast AMPA receptors (AMPA-Rs) and slow NMDA receptors (NMDA-Rs). The synaptic vesicle cycle has several steps. (1) vesicle replenishment, (2) docking, (3) priming, (4) exocytosis, (5) endocytosis, and (6) synaptic vesicle recycling. For details, see von Gersdorff & Borst (2002); Zucker & Regehr (2002), and Friauf *et al.* (2015).

AMPA receptors mediate fast synaptic transmission at excitatory synapses. AMPA receptors are tetramers composed of the GluR1–4 or GluR A–D subunits. Each subunit exists in two distinct forms, flip and flop. Desensitization occurs much quicker in the flop variants (Koike *et al.*, 2000). NMDA receptors have slow deactivation kinetics, are highly Ca^{2+} permeable, and depolarization is necessary for activation, in order to relieve the channel block by external Mg^{2+}, which happens at resting membrane potential. Deactivation kinetics and Mg^{2+} block depend strongly on the type of GluN2 subunits (Glasgow *et al.*, 2015). NMDA receptors with GluN2A have relatively fast response kinetics (deactivation), decaying within tens of milliseconds. NMDA receptors with GluN2B have slow response kinetics decaying over hundreds of milliseconds. The GluN2B subunit is expressed dominantly at auditory synapses during early development, while GluN2A subunit is expressed at more matured synapses (Sanchez *et al.*, 2015).

Katz and colleagues have proposed the quantal hypothesis, which states that the efficacy of synaptic transmission upon arrival of an action potential depends on three main factors: the number of release sites (N), the postsynaptic response caused by transmitter release from a quantal packet of transmitters or a single synaptic vesicle (q), and the probability of neurotransmitter release at each release site (Pr) (Castillo and Katz, 1954). According to the quantal hypothesis, the amplitude distribution of the postsynaptic responses follows a convolution of Poisson statistics with a Gaussian distribution, the latter of which is determined by the fluctuation of single quantal events. This holds when Pr is low. When Pr is high, the amplitude distribution follows a binominal form (del Castillo & Katz, 1954; Neher, 2017). N and Pr are mediated by presynaptic mechanisms such as the number of releasable pool of vesicles (N) as well as the amounts of Ca^{2+} influx and Ca^{2+} sensitivity of the fusion

machinery, which determine Pr. Q is determined by postsynaptic factors such as the sensitivity of postsynaptic receptors to transmitters as well as the number and density of postsynaptic receptors.

1.5.2. Short-term plasticity

The amplitudes of postsynaptic responses change rapidly in an activity-dependent manner, which last over milliseconds to minutes (Friauf *et al.*, 2015). Such short-term synaptic plasticity occurs in most chemical synapses. Repetitive stimulation of presynaptic neurons facilitates or depresses synaptic responses. Short-term synaptic plasticity supports various types of neural computations (Regehr & Abbott, 2004). For example, short-term plasticity is able to act as gain control and operates as a filter of the information flow between neurons (von Gersdorff & Borst, 2002).

The valence of short-term plasticity (facilitation vs depression) is determined by the initial release probability. Synapses with a high initial release probability tend to depress, whereas those with a low initial probability usually facilitate (Zucker & Regehr, 2002; Regehr, 2012). The mechanisms of short-term depression and facilitation are diverse (Fig. 4). For depression, Ca^{2+} channel inactivation and depletion of the readily-releasable pool of synaptic vesicles are the two major presynaptic mechanisms. In addition, a failure of action potential invasion, the slowing of synaptic vesicle replenishment, and the inactivation of release sites though delayed clearance of released materials due to slow endocytosis may be responsible, too. For postsynaptic mechanisms, the desensitization of postsynaptic receptors is a major mechanism at particular synapses. For synaptic facilitation, Ca^{2+} channel facilitation, broadening of action potentials, accumulation of residual Ca^{2+}, activation of the facilitation sensor, and saturation of endogenous Ca^{2+} buffers are

candidate mechanisms (Regehr, 2012). Quantitative analyses are necessary to dissect the precise mechanisms of short-term plasticity.
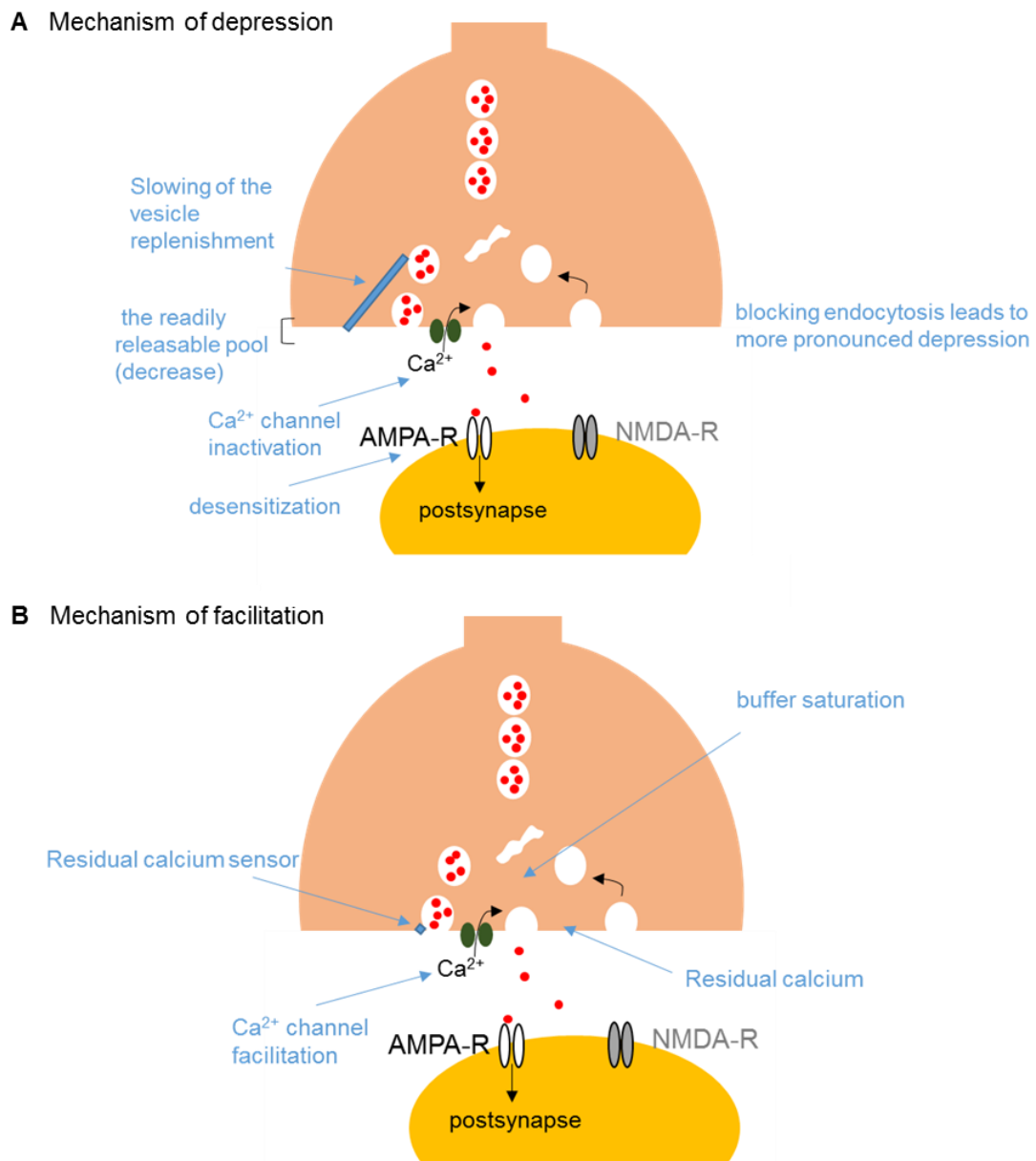
Figure 4. The factors relevant to short-term plasticity
(A) Schematic illustrating mechanisms of depression. (B) Schematic illustrating mechanisms of facilitation. For details, see von Gersdorff & Borst (2002), Zucker & Regehr (2002), and Regehr (2012).

1.6. Synaptic responses of CNIC neurons mediated by ionotropic receptors.

Whole-cell voltage-clamp recordings from CNIC neurons revealed mixed inhibitory and excitatory postsynaptic responses upon direct stimulation of the LL and the CoIC (Moore *et al.*, 1998; Vale & Sanes, 2002; Vale *et al.*, 2004; Sivaramakrishnan & Oliver, 2006; Yassin *et al.*, 2016; Moore & Trussell, 2017). The excitatory postsynaptic responses consist of fast and slow responses mediated by AMPA and NMDA receptors, respectively (Wu *et al.*, 2004). The inhibitory postsynaptic responses are mediated by GABA$_A$ and glycine receptors (Moore *et al.*, 1998; Wu *et al.*, 2004; Moore & Trussell, 2017). Although these studies revealed basic synaptic properties, many studies focus on the synaptic properties before hearing onset, while developmental changes of synaptic responses, especially around the time of hearing onset remain to be investigated.

1.7. Developmental changes of synaptic plasticity in the auditory pathway.

Hearing onset occurs around postnatal day 12 (P12) in rodents when the auditory canals open (Schneggenburger & Forsythe, 2006). Before hearing onset, spontaneous neural activity is necessary for forming proper auditory circuits such as synapse wiring (Clause *et al.*, 2014; Wang & Bergles, 2015). Although acoustic inputs are not necessary for synapse wiring, they dramatically change synaptic properties at a given synapse. After the onset of hearing, bilateral deafness alters synaptic properties at the calyx of Held in the auditory brainstem. For example, the downregulation of postsynaptic NMDA receptors depends on acoustic activity (Futai *et al.*, 2001). In addition, synaptic strengths are altered by hearing loss (Erazo-Fisher *et al.*, 2007). Thus, the functional maturation or fine-tuning of auditory synapses relies to a large extent on acoustic inputs.

1.7.1. The calyx of Held synapse is a model synapse of developmental maturation in the auditory pathway.

The calyx of Held (Fig. 5), which is located in the auditory brainstem, is a large glutamatergic nerve terminal that innervates a single principal neuron of the medial nucleus of the trapezoid body. The calyx synapse has been used as a model system for studying developmental changes of synaptic properties, by taking advantage of the large pre- and postsynaptic compartments that allow simultaneous electrical recordings (Taschenberger & von Gersdorff, 2000; Brenowitz & Trussell, 2001; Iwasaki & Takahashi, 2001; Joshi & Wang, 2002; Magnusson *et al.*, 2005; Kim & Kandler, 2010; Crins *et al.*, 2011). These studies revealed remarkable changes around the onset of hearing. In particular, presynaptic action potentials follow high-frequency stimulation up to a kHz range. Furthermore, the combination of a large synaptic vesicle pool and the reduced release probability of synaptic vesicles at the presynaptic side ensure less short-term synaptic depression and hence reliable synaptic transmission during high-frequency firing. At the postsynaptic side, NMDA receptors are downregulated and the AMPA receptor isoforms exhibit fast activation and deactivation kinetics. These features provide the cellular basis of circuit adaptation to high-frequency auditory signaling up to a kHz range. The functional parameters during synaptic maturation (before and after the onset of hearing) are summarized in Table 1.
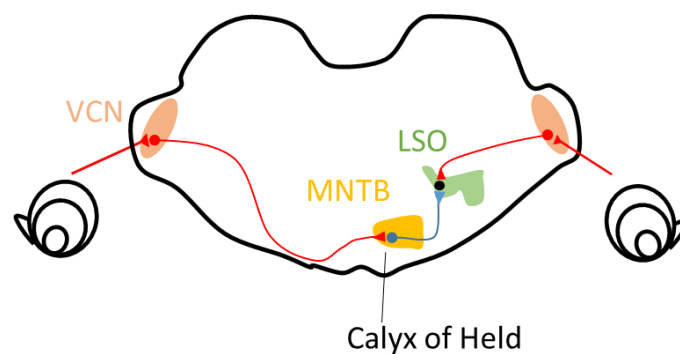
Figure 5. The calyx of Held is a giant glutamatergic synapse.
The calyx of Held terminal terminates on the MNTB neurons. The neurons in the LSO, next station See von Gersdorff & Borst (2002) and Schneggenburger & Forsythe (2006) for details.

Table 1. Summary of the maturation of synaptic properties at the calyx of Held.
Various functional properties which have been changed during maturation are described.   See von Gersdorff & Borst (2002), Schneggenburger & Forsythe (2006), and Steinert et al. (2010) for details.

	Calyx of Held	
	before hearing onset	after hearing onset
Morphology	Spoon-shaped structure	Multidigit-like structure
Presynaptic AP waveform	Faster with development	
Release probability	Reduce release probability	
The readily releasable pool of vesicles	Larger with development	
Ca^{2+} channel subtypes	Mixture of R, N and P/Q Ca^{2+} channels	P/Q subtype
The amplitude of AMPA receptor mediated EPSC	Increase in the amplitudes or similar	
The amplitude of NMDA receptor-mediated EPSC	Decrease in the amplitudes	
The decay kinetics of AMPA receptor-mediated EPSC	Acceleration with development	
The decay kinetics of NMDA receptor-mediated EPSC	Acceleration with development	
Short-term plasticity	Decrease in synaptic depression with age	

1.7.2. Developmental changes of synaptic wiring in the IC.

CNIC cells are generated at embryonic day 14 and some afferent axons from the CN reach the IC at embryonic day 17–18 in rats (Brunso-Bechtold & Henkel, 2005). The basic pattern of afferent inputs from DNLL to the CNIC is already present around birth or latest by P4 in rats. The refinement of auditory ascending projections continues until the onset of hearing (Gabriele *et al.*, 2000; Brunso-Bechtold & Henkel, 2005).

Around the onset of hearing (around P12), CNIC neurons respond transiently to tone stimulation. After P15, some CNIC neurons start to respond reliably to tones in rats and the response

is similar to that in adults (Clopton & Winfield, 1976; Shnerson & Willott, 1979; Grécová *et al.*, 2009), indicating that the properties of input synapses may be developmentally regulated to secure reliable transmission. Although developmental changes in the intrinsic connectivity within the CNIC have been studied on a cellular level (Sturm *et al.*, 2014), those of the input synapses have not yet been examined quantitatively.

1.8. Aims of this thesis

In this study, I focused on the functional properties of synaptic transmission in the CNIC. The CNIC is the major auditory relay station in the mammalian midbrain. The CNIC integrates the ascending information from almost all lower brainstem nuclei as well as commissural connections between the contralateral IC. I examined how developmental changes of synaptic transmission allow reliable information transmission in the CNIC by focusing on excitatory synapses that provide inputs to the CNIC. Although previous studies have shown that synapses in the lower auditory relay stations, such as the calyx of Held, are developmentally optimized for fast signaling, little is known about developmental changes in the CNIC. In particular, developmental changes of two major inputs, ascending fibers from the lower brainstem (LL pathway) and commissural inputs from the CoIC pathway will be compared. Such information is necessary to understand how the neural circuits in the IC are adapted to sound information on a cellular level.

The overall goals of my thesis are as follows.

1. To characterize the developmental regulation of the synaptic responses mediated by AMPA and NMDA receptors in the CNIC.

2. To investigate the functional properties of synaptic transmission in the CNIC, I compared short-term plasticity of excitatory synapses in the LL and CoIC pathways at near-physiological temperature.

2. Materials and Methods

2.1. Slice preparation

All procedures, including animal experiments were performed in accordance with the guidelines of the Physiological Society of Japan and Doshisha University and were approved by the local committee for handling experimental animals at Doshisha University. Male and female Wister rats aged P9-11 and P15-18 were deeply anaesthetized by inhalation of isoflurane, and after decapitation brains were removed. Coronal brain slices through the IC (300 μm in thickness) were obtained using a Leica VT1200S slicer (Leica, Micro systems, Wetzlar, Germany) in cold oxygenated solution containing (mM): 60 NaCl, 130 sucrose, 2.5 KCl, 25 glucose, 25 $NaHCO_3$, 1.25 NaH_2PO_4, 0.5 ascorbic acid, 3 myoinositol, 2 sodium pyruvate, 0.1 $CaCl_2$ and 3 $MgCl_2$ (pH 7.4, gassed with 95% O_2 and 5% CO_2). For preparing slices from P15-18 rats, NaCl was replaced by sucrose. Each slice contained the IC and visible fibers from the LL and CoIC to the IC. In order to allow the slices to recover from the cutting procedure, they were incubated at 37°C for 1-3 hours in artificial cerebrospinal fluid (ACSF; in mM: 125 NaCl, 2.5 KCl, 2 $CaCl_2$, 1 $MgCl_2$, 25 glucose, 25 $NaHCO_3$, 1.25 NaH_2PO_4, 0.4 ascorbic acid, 3 myo-inositol, and 2 sodium pyruvate; pH 7.4; gassed with 95% O_2, 5% CO_2).

2.2. Electrophysiology

For recordings, slices were continuously superfused in the recording chamber with oxygenated ACSF, or ACSF containing antagonists of postsynaptic receptors, at 30-34°C, and were visualized on

an upright microscope (BX-51, Olympus, Tokyo, Japan) equipped with a water immersion objective (x60, NA 0.90, Olympus). Whole cell patch-clamp recording from a neuron in the CNIC was performed using an EPC-10/2 amplifier (HEKA, Lambrecht, Germany) controlled by PatchMaster software (HEKA) in voltage- or current- clamp mode. Recordings were obtained with patch pipettes of 3.5-6 MΩ resistance made from borosilicate glass microcapillaries (Fig. 6) (1.5 mm open diameter, Harvard). Pipettes were filled with an intracellular solution containing (in mM): 140 K-gluconate, 20 KCl, 10 HEPES, 5 Na_2-phosphocreatine, 5 MgATP, 0.5 NaGTP and 0.5 K-EGTA (pH 7.2). 5 mM QX-314 bromide was added to the internal solution to block Na channels. Series resistances were generally 10-30 (typically 15) MΩ and were compensated by 0-30%. The series resistance error could distort the amplitudes and kinetics of the recorded current. Furthermore, it could distort the synaptic depression ratio when the evoked currents were temporally overlapping. Synaptic responses were elicited with electrical stimuli (100 μs square pulses) and were delivered through bipolar tungsten electrodes (separated by approximately 1 mm) driven by stimulators (A.M.P.I, Jerusalem, Israel; or A-M Systems, USA). Stimulating electrodes were placed in the afferent pathways from LL, and the CoIC (Fig 8A), which followed the procedure of Moore et al. (1998). The stimulus required to produce maximal afferent currents was determined by the stimulus-response curves (the input-output curve; I-O curve). The I-O curve plots the relationship between stimulation intensity and synaptic current amplitudes. Stimulation strengths were 10-50 V, usually around 30 V. Stimulus trains were applied every 10 sec. I-O curve was usually continuous and was not all-or-none manner, suggesting that multiple fibers were stimulated in our conditions. At > 30 V, synaptic responses became relatively reliable and I adjusted the voltage so that it was strong enough to evoke reliable responses. I did not

notice changes of the threshold of stimulus intensity eliciting synaptic responses before and after onset of hearing (Fig. 7) (LL:10.4 ± 3.8 V vs 8.0 ± 2.9 V, CoIC: 15 ± 5 V vs 16.3 ± 4.7 V, n = 3-5), suggesting that fiber excitability was not changed drastically in the developmental range studied here. The liquid junction potential between the pipette and the external solution was not corrected. Measurements of postsynaptic currents (PSCs) were performed in whole-cell voltage-clamp mode. Voltage-clamp recordings were made at a membrane holding potential (Vhold) of -40 mV. Some cells were held at -50 mV, but the data were similar to the ones at -40 mV, and the data were pooled together. To assess short-term plasticity, 5 pulses of repetitive stimulation were applied extracellularly at frequencies of 10, 20, or 50 Hz. GABA$_A$ and glycine receptors were blocked by adding 50 or 100 μM picrotoxin and 2 μM strychnine to the ACSF, respectively. In some recordings, NMDA receptors were blocked by 25 or 50 μM D-(-)-2- Amino-5-phosphonopentanoic acid (D-AP5). D-AP5 and QX-314 bromide were obtained from Tocris Cookson (Bristol, UK). NBQX disodium salt (NBQX) was obtained from Abcam (Cambridge, UK). Other reagents were obtained from Nakalai Tesque (Kyoto, Japan). PSCs in ACSF and excitatory postsynaptic currents (EPSCs) in the presence of receptor antagonists were averaged over 5-20 sweeps. Inhibitory postsynaptic currents (IPSCs) were extracted by comparing the traces in the presence and absence of picrotoxin. NMDA receptor-mediated EPSCs (NMDA-EPSCs) were extracted by applying NBQX.

The EPSC amplitudes were measured as the difference between the peak amplitude and the extrapolated exponential decay of the previous EPSC. The EPSC decay time constants were obtained by fitting with a single exponential. For the analysis of the decay, I avoided using multisynaptically evoked responses. Namely, I examined each EPSC and only analyzed visually single-peak synaptic

responses. For monosynaptic AMPA-EPSCs, I considered that the time to peak was usually within 5 ms. For NMDA-EPSCs, time to peak was slower because of slow receptor activation (usually ~10 ms), but eliminated clearly multi-peaked responses. I should note that I have used fibre stimulation and cannot entirely exclude the possibility of multi-synaptic responses. Data were pooled from synaptic responses irrespective of cell types, because I did not detect any differences in synaptic properties among cell types. Firing patterns were analyzed according to their response to 500 ms (negative and positive) current injections with varied amplitudes (from -200 to +700 pA by a 100 ms step). In previous studies using depolarizing current injections, cell types were classified as regular, adapting, or transient types. By using responses to hyperpolarizing or pre-hyperpolarizing currents, cell types were classified as rebound, non-rebound, or pause-build types (Sivaramakrishnan & Oliver, 2001, 2006; Koch & Grothe, 2003).
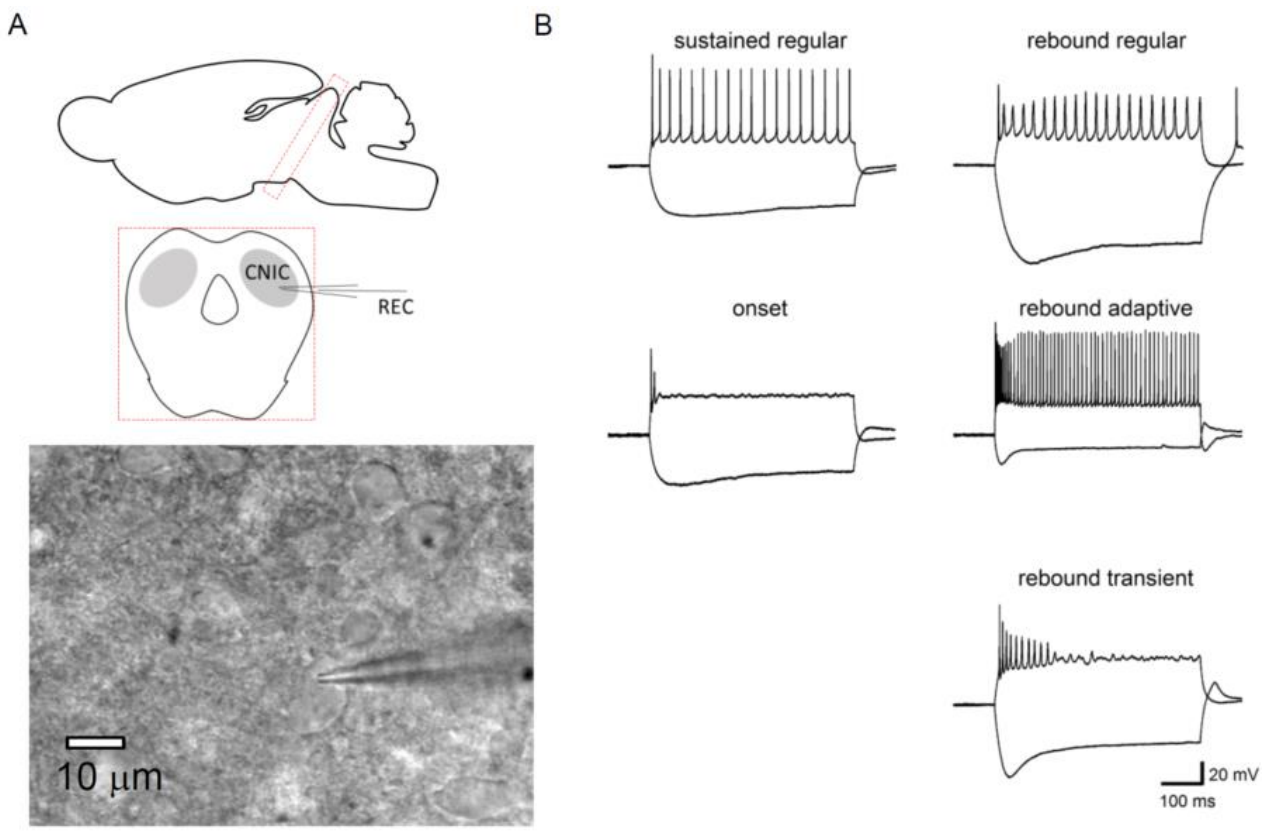
Figure 6. Whole-cell patch clamp recording
(A) Whole-cell recordings from the CNIC neuron. The glass pipette are used for whole cell clamp of the CNIC

20

neuron. Coronal brain slices (300 μm) containing in the CNIC. (B) The firing patterns of cell types were classified according to the previous studies. In this panel, firing patterns are classified into 5 types.
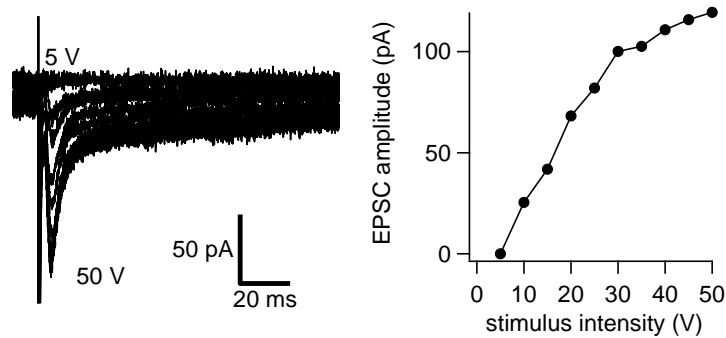
Figure 7. LL-evoked postsynaptic currents recorded in CNIC neuron to single pulse stimulation.
Recording was performed in the whole-cell voltage clamp mode. In Left and Right, pharmacologically isolated EPSCs recorded from one CNIC neuron and representative stimulus-response curve is shown, respectively. The increase was gradual but not all-or none, suggesting that multiple fibers were stimulated.

2.3. Data analysis

Data were acquired at a sampling rate of 20 kHz, after low-pass filtering at 2.9 or 6 kHz. Data were analyzed by IGOR Pro 6.22A (WaveMetrics, Lake Owswego, OR, USA), and MS Excel 2010 software (Microsoft). Statistical significance was assessed using Student's t tests, Welch's t tests, and three-way ANOVAs with post hoc multiple comparisons (Tukey- Kramer method), using statistical software (Excel or R version 3.3.3). When I applied three-way ANOVA, I first did ANOVA analysis for two pathways (LL and CoIC), three frequencies (10, 20, 50 Hz) and five stimuli, or else, two age groups, three frequencies and five stimuli. After this, I performed post-hoc comparisons for comparing each parameter (pathway-dependence, differences in the time courses) using Tukey-Kramer method. In order to examine whether statistical results are robust, I have also performed 3-way mixed ANOVA, in which I considered that stimulus train was obtained from the same cell. However, the results are basically the same ($p < 0.05$) for the main findings of the study. Data were

considered statistically significant when $p < 0.05$. Data are presented as mean ± SEM.

3. Results

3.1. Firing pattern of CNIC neurons

Among 20 cells measured before the onset of hearing, 32% were sustained-regular type, 37% were onset type, 11% were rebound-regular type, 5% were rebound-adapting type, and 16% were rebound-transient type. Among 17 neurons measured after the onset of hearing, 35% were sustained-regular type, 12% were onset type, approximately 18% were rebound-regular type, 24% were rebound-adapting type, and approximately 12% were rebound-transient type. The pause-build firing pattern was not identified in this study, because we did not apply pre-hyperpolarization current pulse. Data was pooled from synaptic responses irrespective of cell types, because I did not detect any differences in synaptic properties among cell types.

3.2. Synaptic responses of CNIC neurons in response to extracellular stimulation of LL and CoIC in P9-11 rats.

I have characterized the synaptic currents in response to electrical stimulation of the LL or CoIC using acute coronal brain slice preparations from rats (P9–11). The LL or CoIC pathways were stimulated extracellularly (Figure 8A). Figure 8B shows example traces of LL- and the CoIC-evoked PSCs in response to a single stimulus. The LL-evoked PSC was inward and the CoIC-evoked PSC was outward in this example, and the LL-and CoIC-evoked EPSCs were isolated by application of picrotoxin. GABAergic currents were extracted by comparing the responses in the presence and absence of picrotoxin. The EPSC amplitudes were measured in extracellular solution containing

either only picrotoxin (LL, $n = 7$; CoIC, $n = 7$), or picrotoxin and strychnine (LL, $n = 26$; CoIC, $n = 21$). In the LL pathway the EPSC amplitudes with and without strychnine were 358.6 ± 70.6 pA ($n = 26$) and 261.4 ± 84.9 pA ($n = 7$, $p = 0.50$ from t-test, Table 2), respectively. In the CoIC pathway, they were 151.1 ± 26.3 pA ($n = 21$) and 243.3 ± 73.6 pA ($n = 7$, $p = 0.15$ from t-test, Table 2), respectively. Because of the data scatter, I could not detect the difference between the two conditions. I have used extracellular stimulation, and it is not straightforward to compare the two conditions obtained from different cells. Indeed, it is well established that glycinergic IPSCs are observed at this preparation (Moore et al., 1998; Choi Buentello, Bishop, & Oliver, 2015; Moore & Trussell, 2017). Nevertheless, the main purpose of this study is to analyze the EPSCs. On average, the amplitudes of the LL-evoked EPSCs and CoIC-evoked EPSCs were 338.0 ± 58.3 and 174.1 ± 27.3 pA, respectively in our conditions (LL, $n = 33$; CoIC, $n = 28$, Table 2). Again, it is not straightforward to compare the EPSC amplitudes between two pathways because I have used extracellular fibre stimulation for evoking EPSCs. In Figure 8C, AMPA receptor-mediated (AMPA-) EPSCs were isolated by applying D-AP5 (25 or 50 μM), an NMDA receptor antagonist. The slow component was reduced, consistent with blockage of NMDA receptors (LL, $n = 11$; CoIC, $n = 7$, for further quantification, see Figure 9). Conversely, when the AMPA-EPSCs were blocked by NBQX (10 μM), the slow component remained, which is likely to be indicative of NMDA-EPSCs (Figure 8D, LL, $n = 7$; CoIC, $n = 9$).
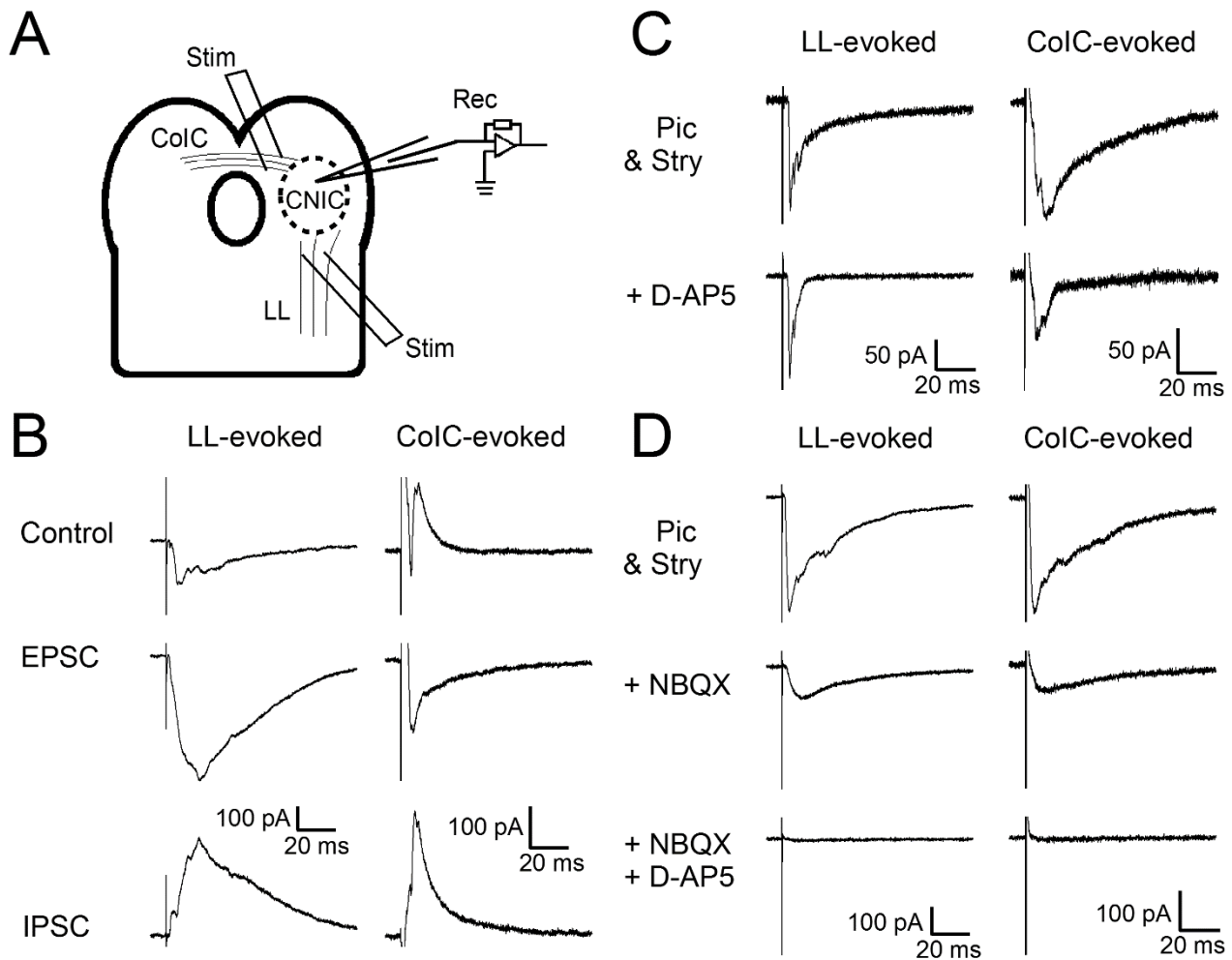
Figure 8. Lateral lemniscus (LL)- and commissure of the inferior colliculus (CoIC)-evoked postsynaptic currents (PSCs) have excitatory and inhibitory components.

(A) Schematic view of the experiments. Neurons in the central nucleus of the inferior colliculus were patch-clamped at V_{hold} = -40 mV. The LL- or CoIC-pathways was stimulated extracellularly by bipolar stimulation electrode. The LL-evoked (left) and the CoIC-evoked (right) currents under different conditions are shown in B-D.

(B) Top traces: Control responses were recorded with the brain slice perfused in normal ACSF. Middle traces: The EPSCs were recorded in the presence of picrotoxin (50-100 µM). Bottom traces: IPSCs were extracted by comparing the responses in the presence (middle traces) and absence (top traces) of picrotoxin.

(C) Similar to B, but the traces with (bottom traces) and without (top traces) D-AP5 are shown. Picrotoxin and strychnine were always present.

(D) Similar to B, but the traces under control conditions (top traces), in the presence of NBQX (middle traces), and in the presence of NBQX and D-AP5 (bottom traces) are shown.

Table 2. Comparison of the EPSC amplitudes between LL and CoIC at P9–11

EPSC (P9-11)	n	amplitude (pA)			t-test
LL (picrotoxin)	7	261.4	±	84.9	p=0.50
LL (picrotoxin+strychinine)	26	358.6	±	70.6	
CoIC (picrotoxin)	7	243.3	±	73.6	p=0.15
CoIC (picrotoxin+strychinine)	21	151.1	±	26.3	
LL summary (mix)	33	338.0	±	58.3	p < 0.05
CoIC summary (mix)	28	174.1	±	27.3	

3.3. Developmental changes in the amplitude and decay of the AMPA- and NMDA-EPSCs at synapses from the LL and CoIC pathways.

To examine developmental changes in the EPSC kinetics, the AMPA- and NMDA-EPSCs were compared at the synapses between the following two age groups: P9-11 (before hearing onset) and P15-18 (after hearing onset). The AMPA- and NMDA-EPSCs are presented in Figure 9A and B. The AMPA- and NMDA- EPSCs were isolated by applying D-AP5 (25-50 μM) and NBQX (10 μM), respectively.

The mean amplitudes of LL-evoked AMPA-EPSCs at P9-11 and P15-18 were 186.2 ± 65.2 pA ($n = 11$) and 299.0 ± 79.2 pA ($n = 8$), respectively (no statistical significance, $p = 0.28$ from Student's t-test, Table 3). The amplitudes in the CoIC pathway were 55.9 ± 18.7 pA ($n = 7$), and 125.0 ± 53.0 pA ($n = 6$), respectively (not statistical significance, $p = 0.48$ from Welch's t-test, Table 3). Because I have used extracellular fiber stimulation for evoking EPSCs, it is not straightforward to compare the EPSC amplitudes, although stimulus threshold for evoking EPSCs seemed unchanged during development (see methods). I also monitored developmental changes in the decay time course. The decay of AMPA-EPSCs did not change during development, as shown in Fig 9C. Specifically, the decay time constants of LL-evoked EPSCs were 4.09 ± 0.57 ms ($n = 11$) and 3.13 ± 0.81 ms ($n = 8$)

at P9-11 and P15-18, respectively (no statistical significance from *t*-test, $p = 0.33$, Table 3). The decay of the CoIC-evoked EPSCs were 4.88 ± 0.53 ms and 3.74 ± 0.28 ms, at P9-11 ($n = 7$) and P15-18 ($n = 6$), respectively (no statistical significance from *t*-test, $p = 0.10$, Table 3).

Figure 9D shows an exponential fit to the decay phases of the LL- and the CoIC-evoked NMDA-EPSCs, indicating that the time constant became significantly faster by 37% (LL: 21.8 ± 2.12 ms to 13.8 ± 2.41 ms, $p < 0.05$ from *t*-test, $n = 8$ and 12, respectively) and 34% (CoIC: 38.3 ms $\pm$ 2.54 ms to 25.4 ± 3.63 ms, $p < 0.05$ from *t*-test, $n = 7$ and 7, respectively), respectively, at P15-18 (Table 3). I failed to observe the difference in the mean amplitudes of the NMDA-EPSCs in both pathways. Specifically, the LL-evoked NMDA-EPSC amplitudes were 193.7 ± 49.3 pA and 78.5 ± 15.5 pA at P9-11 and P15-18, respectively (no statistical significance from *t*-test, $p = 0.06$, $n = 8$ and 12, respectively), whereas the CoIC-evoked EPSC amplitudes were 79.1 ± 29.3 pA and 40.0 ± 13.9 pA (no statistical significance from *t*-test, $p = 0.25$, $n = 7$ and 7), respectively (Table 3). I cannot exclude the possibility that NMDA EPSCs were decreased in the LL pathway. However, strong downregulation did not happen at the IC around hearing onset as seen in the calyx of Held (Taschenberger & von Gersdorff, 2000).

In addition, I did not observe changes in the amplitude ratio of the NMDA- to AMPA-EPSCs (P9-11 vs P15-18, no statistical significance from *t*-test LL, $p = 0.23$; CoIC, $p = 0.19$), although the values were variable among cells. The ratios were 0.50 ± 0.08 (LL, $n = 8$) and 0.78 ± 0.24 (CoIC, $n = 7$) at P9-11 (Fig 9E). The NMDA/AMPA ratios at P15-18 were 0.37 ± 0.06 (LL, $n = 12$) and 0.40 ± 0.12 (CoIC, $n = 7$, Table 3). The important point here is that strong downregulation of NMDA-EPSC amplitudes did not occur at the IC, in contrast to the auditory brainstem (Taschenberger & von

Gersdorff, 2000; Futai *et al.*, 2001).
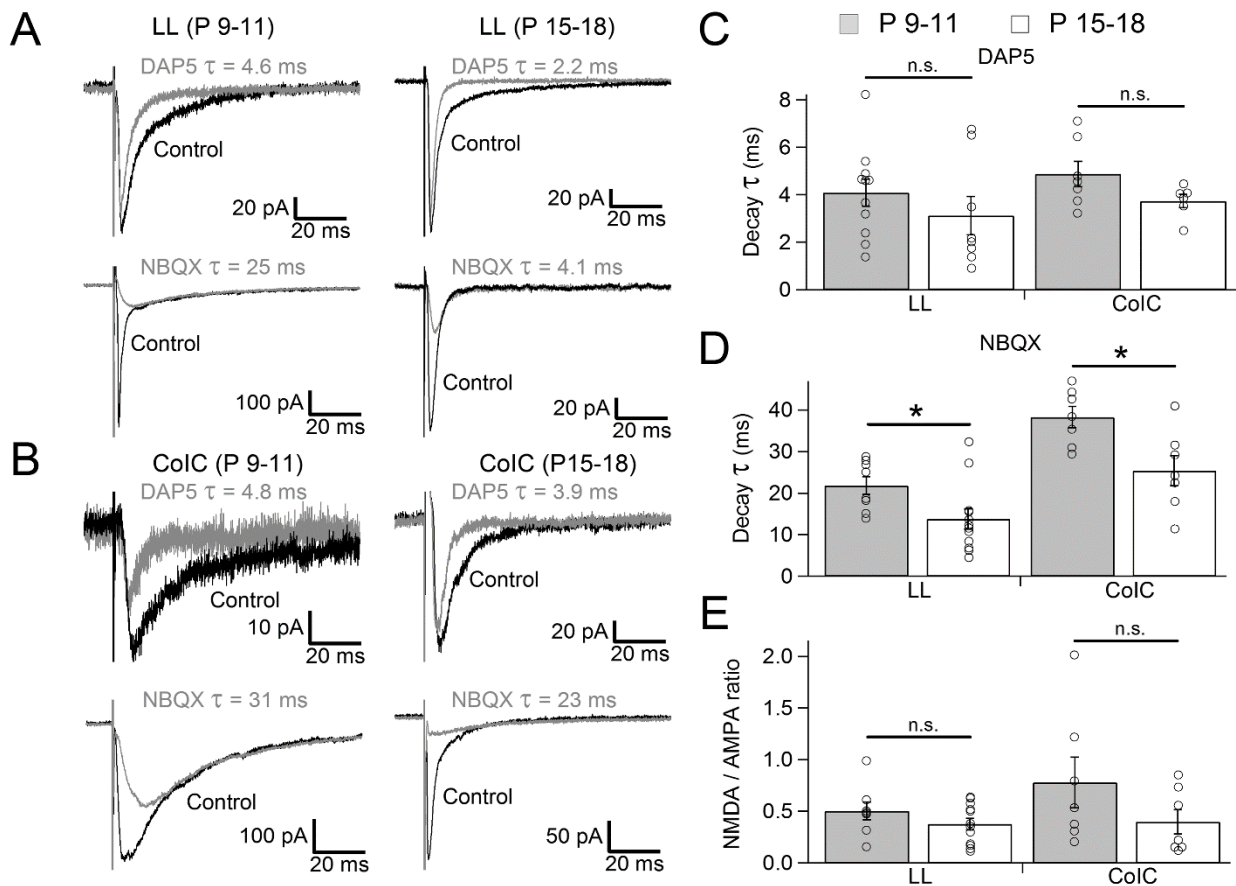
Figure 9. Acceleration of the EPSC decay, but no change in the NMDA/AMPAR ratio after hearing onset.

(A) Top: Example traces of LL-evoked EPSCs recorded before (left) and after (right) the onset of hearing. Control traces (black) and traces in the presence of D-AP5 (grey) are shown. Bottom: Control traces (black) and traces in the presence of NBQX (grey).

(B) The same as A, but CoIC-evoked EPSCs are shown.

(C) The decay time constants of AMPA-EPSC before (grey bars) and after (open bars) the onset of hearing are shown. Left and right show the data of the LL-evoked (P9-11, n = 11; P15-18, n = 8) and the CoIC-evoked (P9-11, *n* = 7; P15-18, *n* = 6) EPSCs, respectively. Both average and individual data are shown.

(D) Similar to C, but the decay time constants of NMDA-EPSC are shown. Left and right show the data of the LL-evoked (P9-11, *n* = 8; P15-18, *n* = 12) and the CoIC-evoked (P9-11, *n* = 7; P15-18, *n* = 7) EPSCs, respectively.

(E) The same as C and D, but the amplitude ratios of NMDA- to AMPA-EPSCs are shown. The same number of cells as D. In C-E, asterisks indicate statistically significant differences: * for $p < 0.05$.

28

Table 3. Decay time constants and amplitudes of the AMPA- and NMDA- EPSCs, and the NMDA/AMPA ratios

			P9-11				P15-18				p-value
LL	AMPA	Decay τ (ms)	4.09	±	0.57	n=11	3.13	±	0.81	n=8	0.33
		amplitude (pA)	186.19	±	65.21		299.00	±	79.21		0.28
	NMDA	Decay τ (ms)	21.81	±	2.12		13.75	±	2.41		0.03
		amplitude (pA)	193.72	±	49.44	n=8	78.52	±	15.53	n=12	0.06
		NMDA /AMPA ratio	0.50	±	0.08		0.37	±	0.06		0.21
CoIC	AMPA	Decay τ (ms)	4.88	±	0.53	n=7	3.74	±	0.28	n=6	0.10
		amplitude (pA)	55.92	±	18.70		125.01	±	52.99		0.26
	NMDA	Decay τ (ms)	38.27	±	2.54		25.39	±	3.63		0.01
		amplitude (pA)	79.07	±	29.28	n=7	39.98	±	13.89	n=7	0.25
		NMDA /AMPA ratio	0.78	±	0.24		0.40	±	0.12		0.19

3.4. Distinct short-term synaptic plasticity of LL- and CoIC- evoked EPSCs and its developmental changes.

I examined short-term plasticity by stimulation of the LL and CoIC at P9-11 rats. EPSCs were isolated pharmacologically by adding picrotoxin (50 or 100 µM; LL, $n = 7$; CoIC, $n = 7$) or picrotoxin + strychnine (2 µM; LL, $n = 16$-17; CoIC, $n = 14$), and the LL or CoIC fibers were stimulated 5 times at 10, 20, or 50 Hz. Figure 10A shows example traces of LL-evoked EPSCs (left traces) and CoIC-evoked EPSCs (right traces) in response to 5 pulses of repetitive stimulation at 10, 20, and 50 Hz. EPSCs were mixtures of AMPA- and NMDA-EPSCs at the holding potential of -40 mV. The amplitudes of LL-evoked EPSCs were depressed at all frequencies. In contrast, CoIC-evoked EPSCs exhibited no depression, and even facilitation at higher frequencies. To determine the extent of short-term synaptic plasticity, the EPSC amplitudes were measured and normalized to the first EPSC in each trace. Figure 11A shows a summary of short-term synaptic plasticity for LL- and CoIC-evoked EPSCs at 10 (LL, $n = 23$; CoIC, $n = 21$), 20 (LL, $n = 23$; CoIC, $n = 21$), and 50 Hz (LL, $n = 24$; CoIC, $n = 21$). The LL-evoked excitatory responses exhibited pronounced short-term synaptic depression (~ 50% of the initial response) at all frequencies. In contrast, the CoIC-evoked responses were constant at 10 Hz and slightly facilitated at 20 and 50 Hz. A significant difference was found between short-term synaptic plasticity at excitatory synapses in the LL and CoIC pathways ($p < 0.001$, $F (1, 635) = 163.3$, ANOVA test) at all frequencies ($p < 0.001$ at all frequencies from post hoc multiple comparisons, see above for the number of cells in each condition, Table 4).

To study developmental changes in short-term synaptic plasticity in response to repetitive stimulation of the LL and CoIC pathways, I recorded EPSCs in response to repetitive stimulation at

P15-18. After the onset of hearing, EPSCs showed slight depression at excitatory synapses in the LL and CoIC pathways. Figure 10B shows example traces of the LL-evoked (left traces) and CoIC-evoked EPSCs (right traces) in response to repetitive stimulation. Compared with P9-11, the amplitude of the LL-evoked EPSCs showed less depression particularly at 50 Hz in Fig 10. In contrast, the short-term plasticity of CoIC-evoked EPSCs did not change drastically, and showed constant responses or slight depression at all frequencies. Figure 11B shows a summary of short-term synaptic plasticity for LL- and CoIC-evoked EPSCs. Both LL-evoked ($n = 20, 23, 18$) and CoIC-evoked ($n = 21, 20$, and 18 for 10, 20, and 50 Hz, respectively). The data scattered in both LL- and CoIC-pathways. On average, EPSCs showed a slight depression or almost constant responses at all frequencies. At the LL pathway, significant differences were observed between two age groups ($p < 0.001$, $F_{(1, 625)} = 80.3$, ANOVA test) when comparing the depression curve at all frequencies ($p < 0.001$ for 10, 20, and 50 Hz, from post hoc multiple comparisons, Table 5). In contrast, no significant difference was observed at the CoIC pathway ($p < 0.001$, $F_{(1, 580)}$, ANOVA test) at any frequencies ($p = 0.94, 0.09$, and 0.34 for 10, 20, and 50 Hz from post hoc multiple comparisons, Table 4). In addition, no significant difference was detected between the two pathways ($p = 0.0044$, $F_{(1, 570)}$, ANOVA test) at any frequencies at P15-18 ($p = 0.77, 0.54, 0.35$ for 10, 20 and 50 Hz, respectively, Table 4), suggesting that both pathways exhibit similar short-term plasticity after hearing onset.
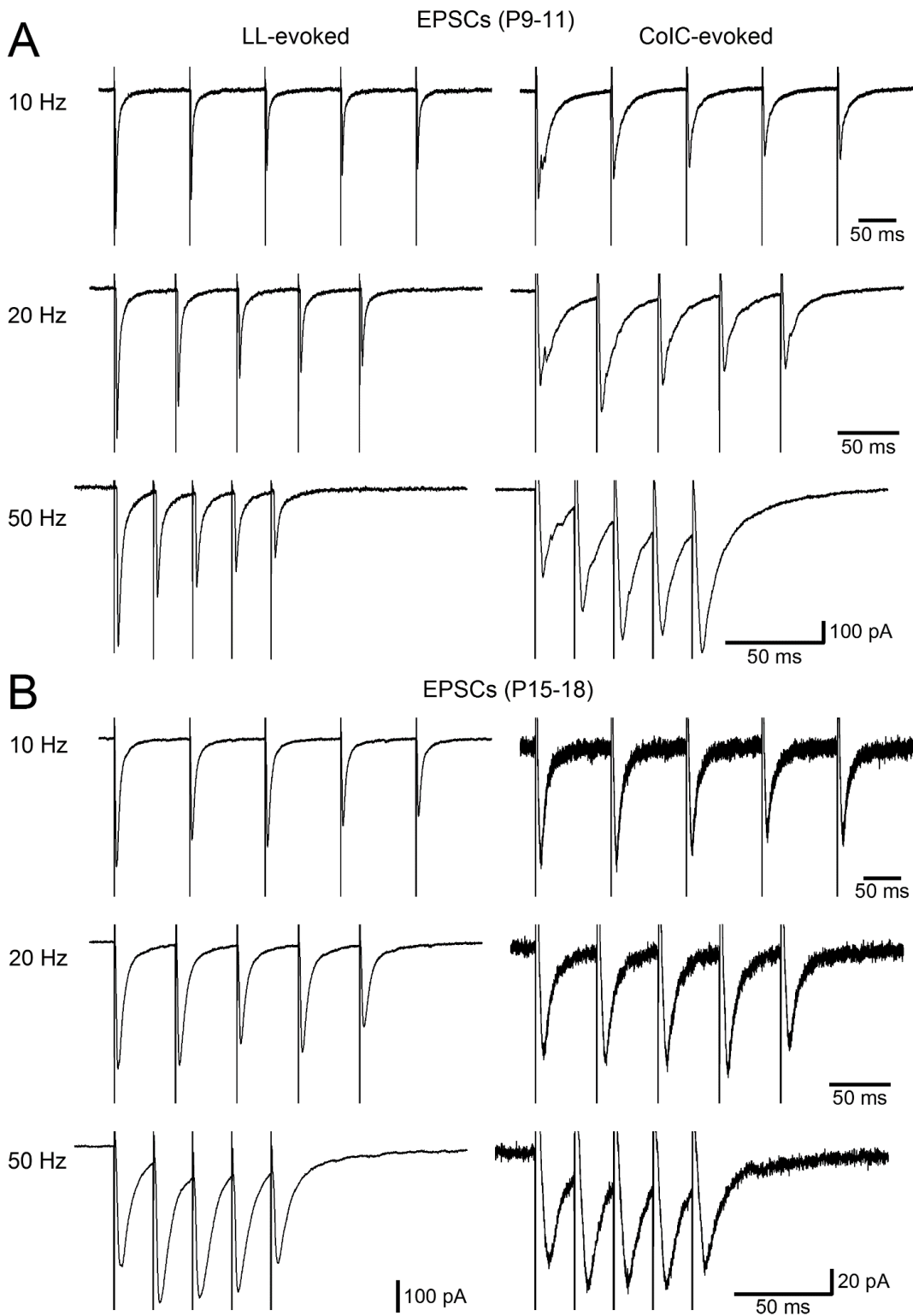
Figure 10. Short-term synaptic plasticity of excitatory synapses evoked by stimulation of the LL and CoIC pathways and its developmental changes.

(A)Representative traces of LL-evoked (left) and CoIC-evoked (right) EPSCs in response to 5 repetitive stimulations. The data were obtained from P9-11 rats. Fibers were stimulated at 10, 20, or 50 Hz (from top to bottom). The extracellular solution contained picrotoxin (50-100 µM) and strychnine (2 µM). Each trace is the average of 10 traces in a given cell.

(B)The same as A, but the data from P15-18 are shown

32

A

P9-11

10 Hz   20 Hz   50 Hz

▲- ColC
○— LL

B

P15-18

10 Hz   20 Hz   50 Hz

▲- ColC
○— LL

C

P8-10 (Vhold = -70mV)

10 Hz   20 Hz   50 Hz

▲- ColC
○— LL

D

P15-18 (Vhold = -70mV)

10 Hz   20 Hz   50 Hz

▲- ColC
○— LL
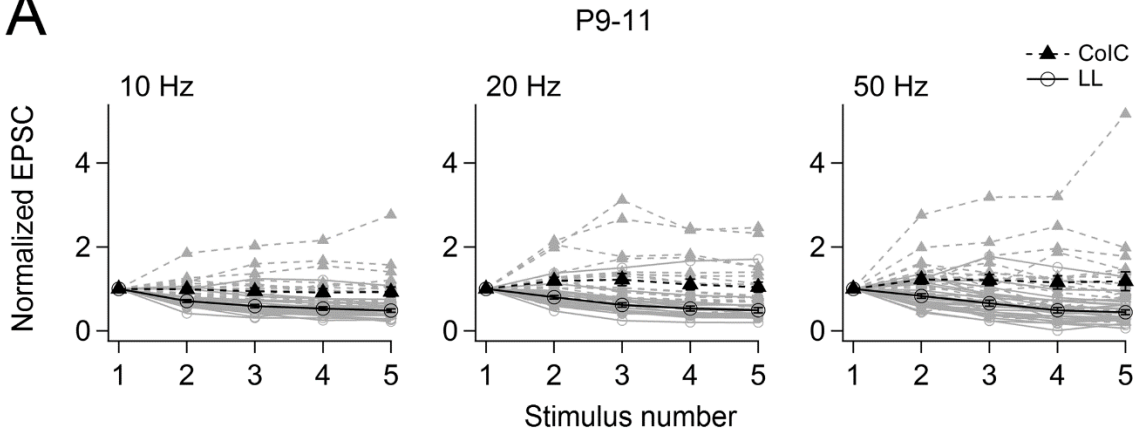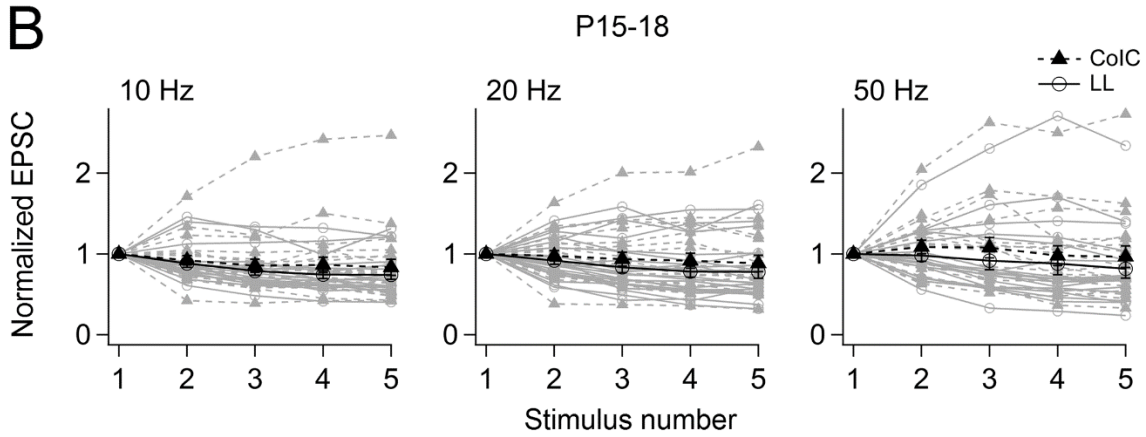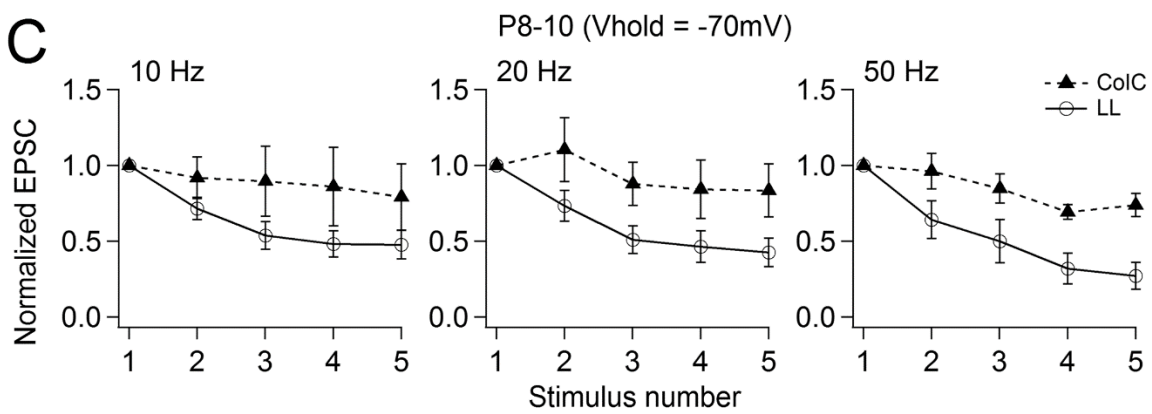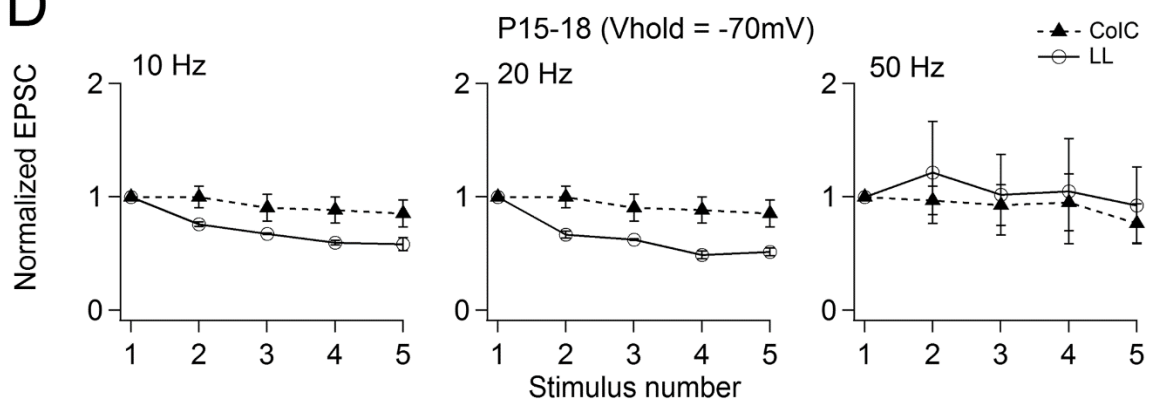
Figure 11. Summary of short-term plasticity of the lateral lemniscus (LL)- (open circles) and CoIC- (filled triangles) evoked excitatory postsynaptic currents (EPSCs).

(A) Summary of short-term plasticity of the LL- (open circles) and CoIC- (filled triangles) evoked EPSCs between P9-11. The EPSC amplitudes were averaged and subsequently normalized to the first one. The data from 10 (left; LL, n = 23; CoIC, n = 21), 20 (middle; LL, n = 23; CoIC, n = 21) and 50 Hz (right; LL, n = 24; CoIC, n = 21) are shown. The average and the individual data are shown as black and grey symbols, respectively. The extracellular solution contained picrotoxin (50–100 μM; LL, n = 7; CoIC, n = 7) or picrotoxin+strychnine (2 μM; LL, 10–20 Hz, n = 16, 50 Hz, n = 17; CoIC, n = 14). Both conditions produced similar results. Significant differences were found in short-term plasticity between the LL and CoIC pathways. (B) Similar to A, but summary of normalized amplitude data from the LL‑ (open circles) and the CoIC‑ (filled triangles) evoked EPSCs between P15–18 is shown. Stimulation frequency was 10 (LL, n = 20; CoIC, n = 21), 20 (LL, n = 23; CoIC, n = 20) or 50 Hz (LL, n = 18; CoIC, n = 18). (C-D) The summary of short-term plasticity of the EPSCs recorded in voltage clamp at −70 mV without D-AP5. Because of negative holding potential, the AMPA-EPSCs should be a major component of the EPSCs. The peak amplitudes were measured by comparing the peak and the baseline just before the stimulus. Exponential fits were not used to extrapolate the baseline level in C and D. The average data are shown as open circles (LL) and filled triangles (CoIC). C shows summary of the normalized amplitudes from the LL and the CoIC-evoked EPSCs at P8–10 rats (10–50 Hz; LL, n = 4-5; CoIC, n = 7-8). D is Similar to C, but the data were obtained from P15-18 rats (10–50 Hz; LL, n = 3-6; CoIC, n = 9).

3.5. Developmental changes in short-term synaptic plasticity of LL- and CoIC-evoked AMPA-EPSCs.

The extent of short-term plasticity is determined by both pre- and postsynaptic factors. If the time course of synaptic plasticity differs between AMPA- and NMDA-EPSCs, it is suggested that postsynaptic factors contribute to the plasticity. For example, AMPA receptors tend to be desensitized during repetitive stimulation whereas NMDA receptors do not (Koike-Tani *et al*., 2007). Conversely, if AMPA- and NMDA EPSCs show a similar time course, presynaptic factors are likely to determine the extent of plasticity. Indeed, by comparing the time course of AMPA- and NMDA-EPSCs during repetitive stimulation, von Gersdorff et al. (1997) suggested that the time course of synaptic depression is determined by presynaptic factors at the calyx of Held. In order to evaluate presynaptic and postsynaptic factors contributing to short-term plasticity, I examined the time course of synaptic

34

depression /facilitation between AMPA or NMDA receptor-mediated EPSCs. Particularly, I have examined whether the differences between LL- and CoIC pathways were mediated by pre- or postsynaptic mechanisms.

In order to examine short-term plasticity of AMPA-EPSCs, NMDA receptors were blocked by D-AP5 (25 or 50 µM) and the AMPA-EPSCs were recorded. Figure 12A shows example traces of LL-evoked AMPA-EPSCs (left traces) and CoIC-evoked AMPA-EPSCs (right traces) recorded from different CNIC neurons in response to repetitive stimulation. The amplitudes of the LL-evoked AMPA-EPSCs were depressed over the period of 5 stimulus pulses at all frequencies. In contrast, there was an increase in the amplitude of CoIC-evoked EPSCs in response to the 2nd stimulus pulse at all frequencies, and other responses were almost constant. Figure 13A shows a summary of short-term synaptic plasticity for LL- ($n = 8, 9, 9$ for 10, 20, and 50 Hz, respectively) and CoIC-evoked ($n = 7, 7, 6$ for 10, 20, and 50 Hz, respectively) AMPA-EPSCs. A significant difference was found between the LL and CoIC pathways ($p < 0.001$, $F (1, 200) = 103$, ANOVA test) at all frequencies ($p < 0.001$ for 10, 20, and 50 Hz from post hoc multiple comparisons, Table 4). Similar results were obtained by holding the membrane potential at -70 mV in the absence of D-AP5, where contribution of the NMDA-EPSCs was supposed to be minor (Figure11C).

I next characterized short-term plasticity of the AMPA- EPSCs after the onset of hearing. Figure 12B and 13B show example traces and a summary of the normalized EPSC amplitudes of the AMPA-EPSCs (LL, $n = 10$; CoIC, $n = 7$), respectively. In the example traces of Fig 12, synaptic depression was less pronounced in the LL pathway whereas slight facilitation was converted to depression in the CoIC pathway in older animals. I should note that the data scatter, as seen in

individual data in Fig 13. Compared with P9-11, the LL-evoked AMPA-EPSCs showed less depression in P15-18 ($p < 0.001$, F (1, 250) = 59.9, ANOVA test) at all frequencies ($p = 0.0016$, $p < 0.001$, $p < 0.001$ for 10, 20, and 50 Hz, respectively from post hoc multiple comparisons, Table 5), whereas CoIC-evoked AMPA –EPSCs remained relatively similar ($p = 0.99$, 0.99, 0.99 for 10, 20, and 50 Hz, respectively with post hoc multiple comparisons, $p = 0.77$. F (1, 175) = 0.089 from ANOVA test, Table 5) on average. In addition, no significant differences were detected between the LL and CoIC pathways ($p = 0.160$, F (1, 225) = 1.99, ANOVA test) at any frequencies at P15-18 ($p = 0.82$, 0.99, and 0.99 for 10, 20 and 50 Hz, respectively from post hoc multiple comparisons, Table 4). Similar results were obtained by holding the membrane potential at -70 mV in the absence of D-AP5, where contribution of the NMDA-EPSCs was supposed to be minor (Figure 11D).
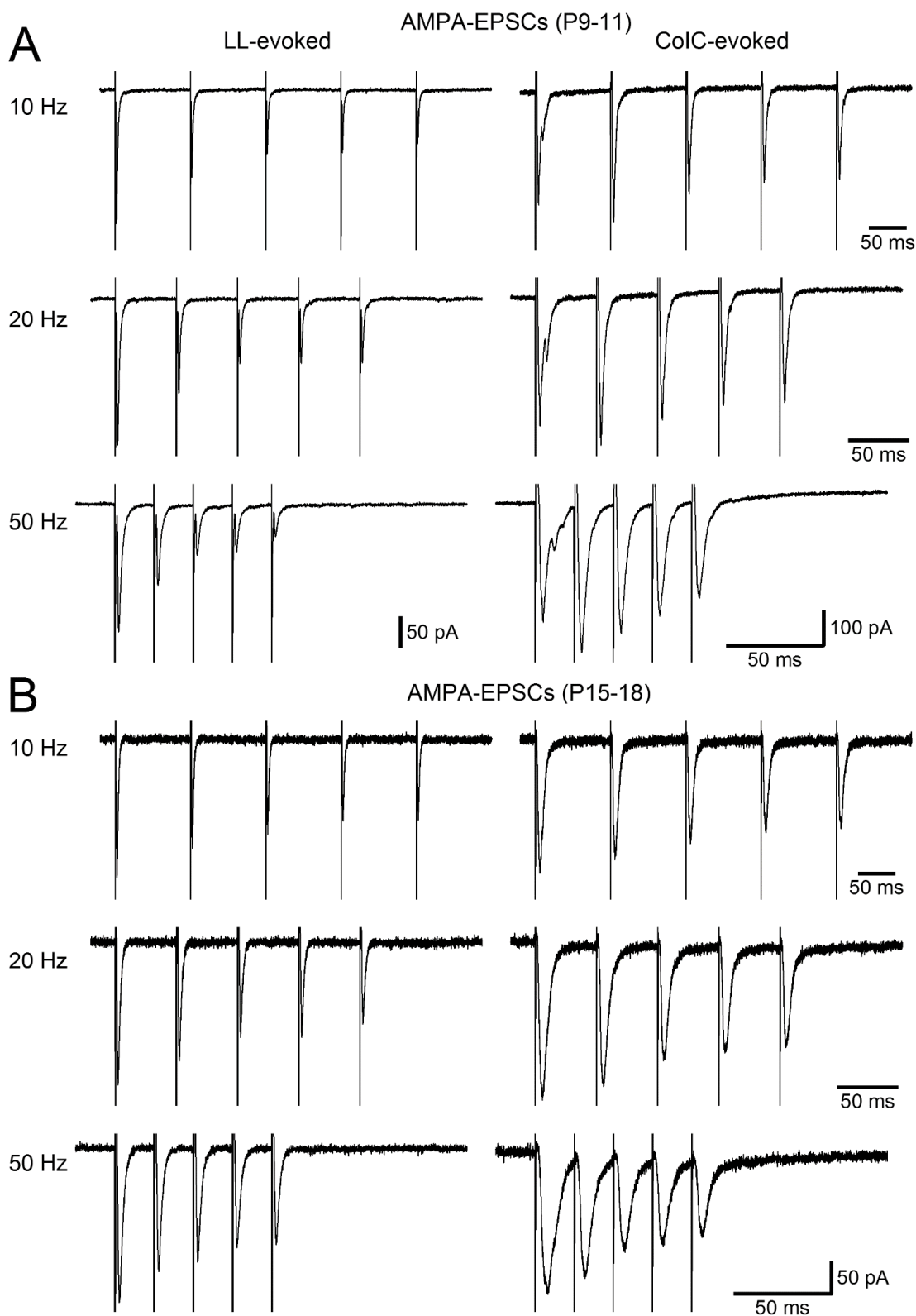
Figure 12. Short-term synaptic plasticity of the AMPA-EPSCs and its developmental changes.
(A) Representative traces of LL-evoked (left) and CoIC-evoked (right) AMPA-EPSCs in response to 5 repetitive stimulations. The data were obtained from P9-11. Fibers were stimulated at 10, 20, or 50 Hz (from top to bottom). The extracellular solution contained D-AP5 (25 or 50 µM) and picrotoxin (50-100 µM), in addition to strychnine (2 µM) in some recordings.
(B) The same as A, but the data are obtained from P15-18 rats.

37
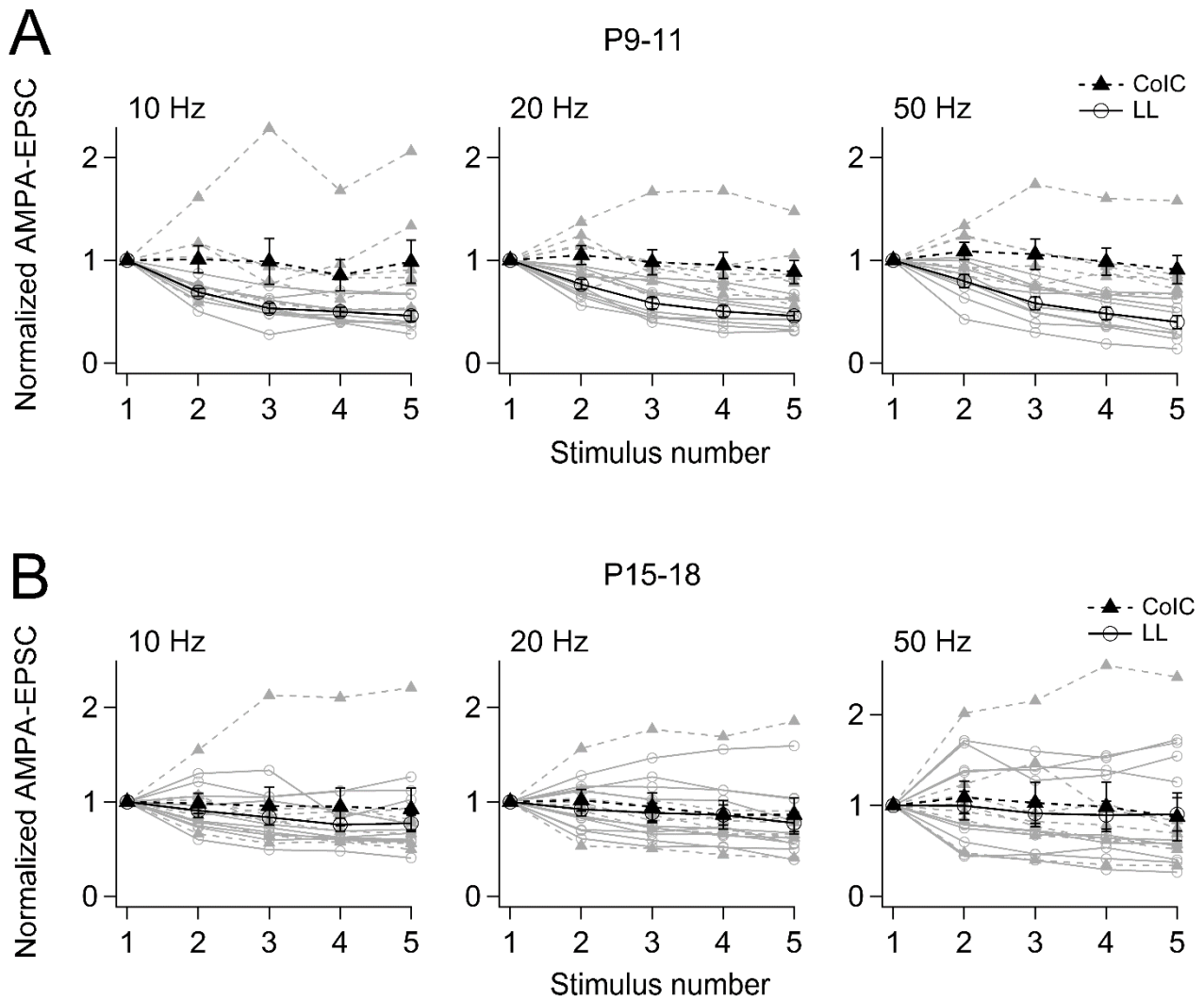
Figure 13. Summary of short-term plasticity of the AMPA excitatory postsynaptic currents (EPSCs).
(A) Summary of short-term plasticity of the LL- (open circles) and CoIC- (filled triangles) AMPA EPSCs at P9–11 rats. Average and individual data are shown as black and grey symbols, respectively. Stimulation frequency was 10 (left; LL, $n = 8$; CoIC, $n = 7$), 20 (middle; LL, $n = 9$; CoIC, $n = 7$) or 50 Hz (right; LL, $n = 9$; CoIC, $n = 6$). (B) Summary of normalized amplitude data from the LL‑ (open circles) and the CoIC‑ (filled triangles) evoked AMPA‑EPSCs (10–50 Hz; LL, $n = 10$; CoIC, $n = 7$) at P15–18 rats.

3.6. Developmental changes in short-term synaptic plasticity of LL- and CoIC-evoked NMDA-EPSCs.

The NMDA receptor-mediated EPSCs were obtained by applying an AMPA receptor antagonist, NBQX (10 µM). Figure 14A shows example traces of LL-evoked NMDA-EPSCs (left traces) and

CoIC-evoked NMDA-EPSCs (right traces) at 10, 20, and 50 Hz obtained from P9-11 rats. Note that some traces in the CoIC pathway had a slow rise, perhaps indicating the voltage clamp issue (synaptic location remote from soma, for example). The amplitude of LL-evoked NMDA-EPSCs decreased over the period of 5 stimulus pulses at all frequencies. In contrast, the CoIC-evoked NMDA-EPSCs stayed constant at 10 Hz or facilitated at 20 and 50 Hz stimulation. Figure 15A shows a summary of short-term synaptic plasticity for LL- ($n = 8$ at all frequency) and CoIC-($n = 9$, 8, and 9 for 10, 20, and 50 Hz, respectively) evoked NMDA-EPSCs. A significant difference between short-term synaptic plasticity of NMDA responses in the LL and CoIC pathways was detected ($p < 0.001$, $F(1, 220) = 194$, ANOVA test) at all frequencies ($p < 0.001$, for 10, 20 and 50 Hz, from post hoc multiple comparisons, Table 4). In addition, the AMPA- and NMDA-EPSCs showed a different time course of depression and facilitation in some conditions. At the LL pathway, no difference was detected at 10 Hz ($P = 0.99$), but differences were detected at 20 and 50 Hz although statistically not large ($P = 0.042$ and 0.047, from post hoc multiple comparisons, for ANOVA test, $p < 0.001$, $F(1, 220) = 11.3$, Table 6). At the CoIC pathway, there was a difference at 20 Hz ($p = 0.008$), but not at other frequencies ($p = 0.54$ and 0.24 for 10 and 50 Hz from post hoc multiple comparisons, $p < 0.001$, $F(1, 200) = 18.1$ from ANOVA test, Table 6). Mismatch between AMPA- and NMDA- EPSCs might suggest postsynaptic mechanism of short-term plasticity (see discussion).

In Fig 14B, short-term plasticity of the NMDA-EPSCs after the onset of hearing (P15-18) was examined. Fig 15B shows a summary of normalized EPSC amplitudes of NMDA-EPSCs (LL, $n = 8$, 11, 8; CoIC, $n = 7$, 6, 7 for 10, 20, and 50 Hz, respectively). Significant difference was detected between the LL and the CoIC pathways at 10 and 20 Hz ($p = 0.007$, and $p < 0.001$), but not at 50 Hz

($p = 0.065$, post hoc multiple comparisons, for ANOVA test, $p < 0.001$, $F(1, 205) = 37.8$, Table 4).

In contrast to AMPA EPSCs, NMDA-EPSCs showed slight facilitation at the CoIC pathway after hearing onset, which explains some difference at certain frequencies. However, the difference was not consistent at all frequencies. Compared with P9-11, the LL-evoked NMDA-EPSCs showed less depression at 10 and 50 Hz ($p < 0,001$ and $p = 0.003$), but not at 20 Hz ($p = 0.13$, post hoc multiple comparisons, for ANOVA test, $p < 0.001$, $F(1, 225) = 37.4$, Table 3) at P15-18, whereas CoIC-evoked NMDA–EPSCs remained relatively similar ($p = 0.99$, 0.37, and 0.72 for 10, 20, and 50 Hz, respectively, post hoc multiple comparisons, for ANOVA test, $p = 0.03$, $F(1, 200) = 4.60$). In the LL pathway, NMDA responses depressed less than AMPA response before hearing onset, which may explain a less pronounced difference between P9-11 and P15-18. After hearing onset, AMPA- and NMDA-EPSCs show a similar degree of depression and facilitation during repetitive stimulation in the LL ($P = 0.99$, 0.99, 0.99 for 10, 20 and 50 Hz with post hoc multiple comparisons, for ANOVA test, $p = 0.75$, $F(1, 255) = 0.10$, Table 6) and CoIC pathways $p = 0.77$, 0.36, 0.85 for 10, 20 and 50 Hz with post hoc multiple comparisons, for ANOVA test, $p = 0.011$, $F(1, 175) = 6.67$, Table 6), suggesting a more important role of presynaptic mechanism of synaptic depression and facilitation.
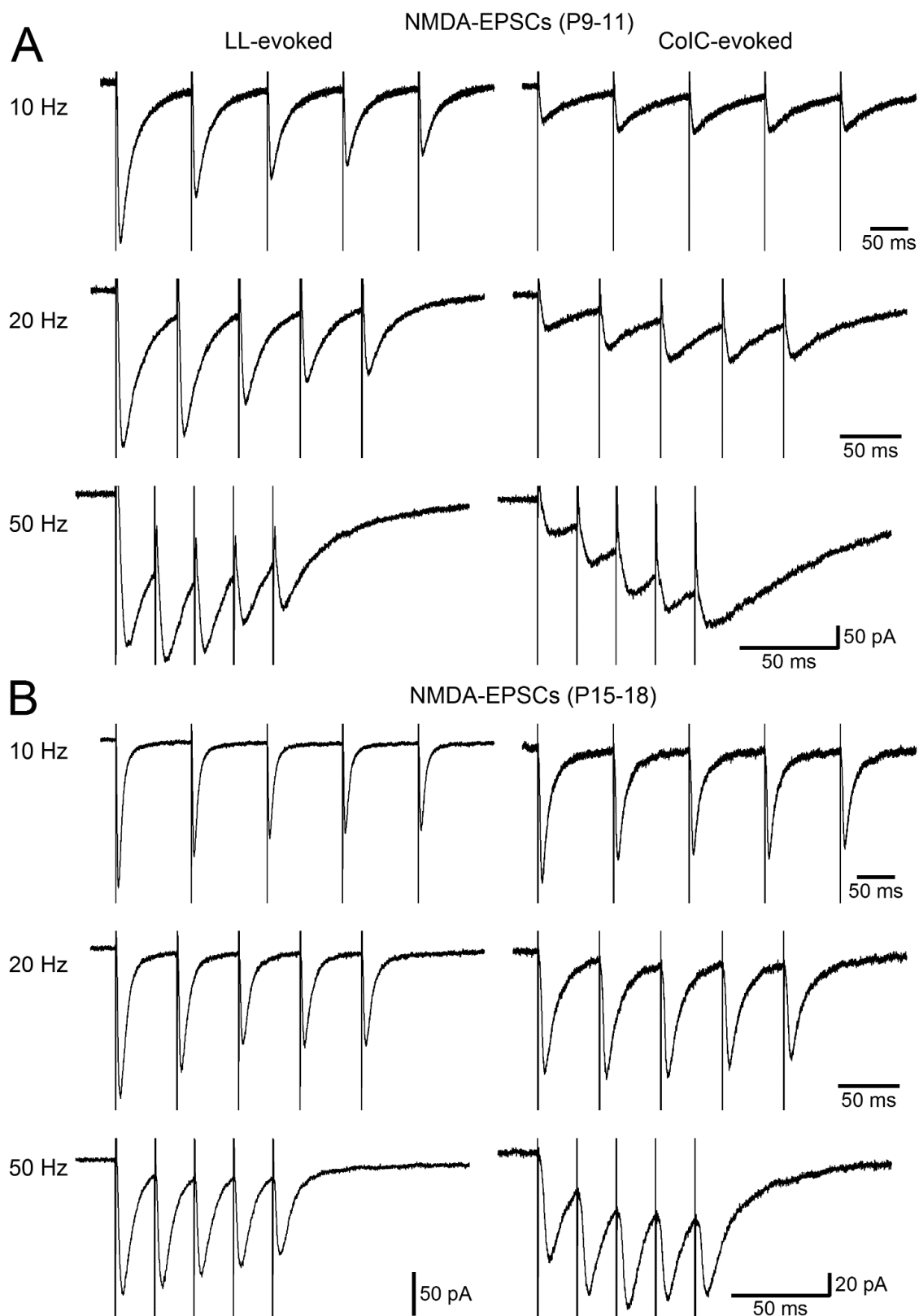
Figure 14. Short-term synaptic plasticity of the NMDA-EPSCs and its developmental changes.

(A) Representative traces of LL-evoked (left) and CoIC-evoked NMDA-EPSCs (right) at 10, 20, or 50 Hz stimulation (from top to bottom) at P9-11 rats. The NMDA-EPSCs were extracted by application of NBQX (10 µM).

(B) The same as A, but the data from P15-18 rats are shown.
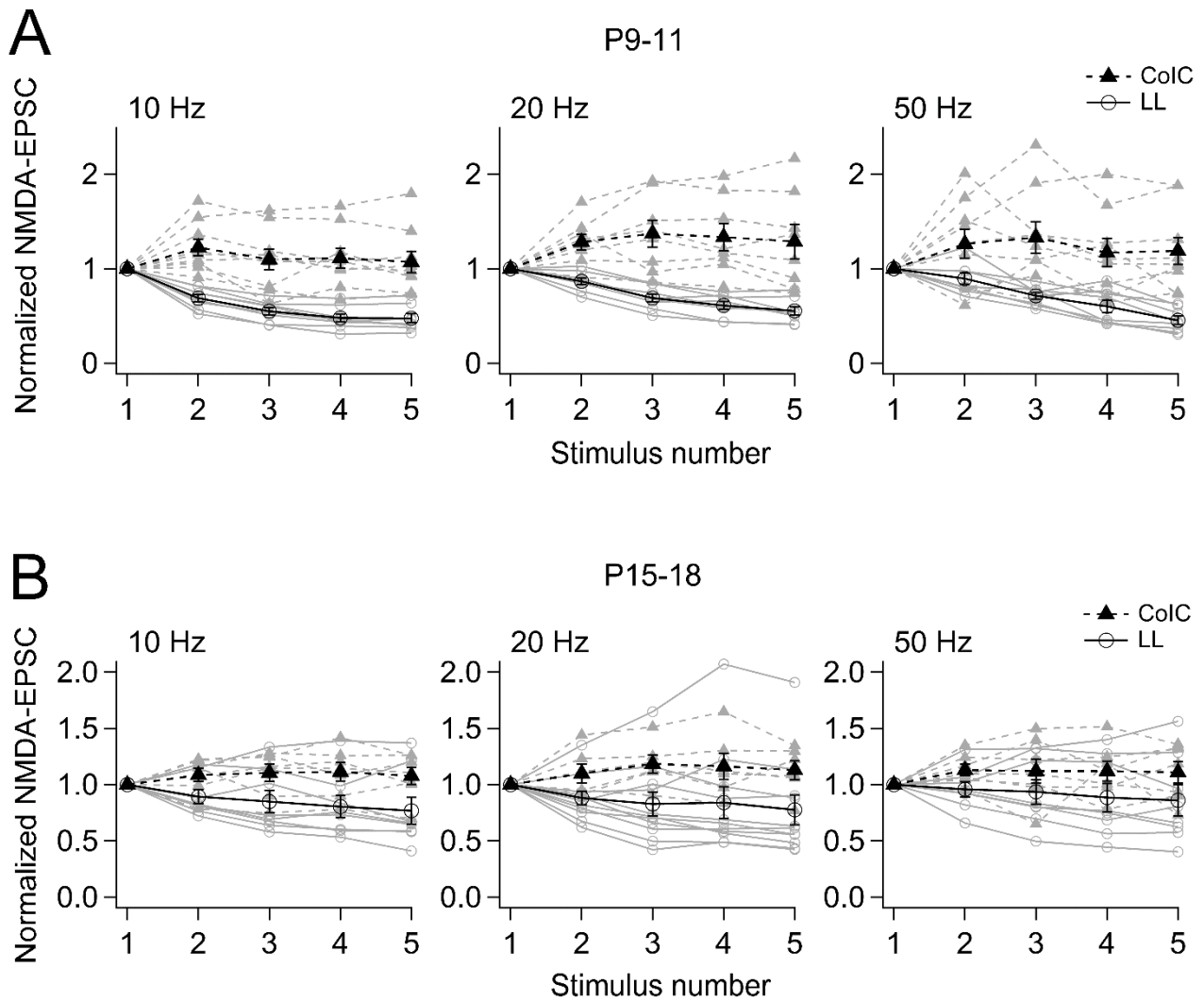
Figure 15. Summary of short-term plasticity of the NMDA-EPSCs.

(A) Summary of short‑term synaptic plasticity for LL (open circles) and CoIC (filled triangles). Stimulation frequency was 10 (left; LL, $n = 8$; CoIC, $n = 9$), 20 (middle; LL, $n = 8$; CoIC, $n = 8$), or 50 Hz (right; LL, $n = 8$; CoIC, $n = 9$). (B) The same as a, but the data from P15–18 rats are shown. Stimulation frequency was 10 (left; LL, $n = 8$; CoIC, $n = 7$), 20 (middle; LL, $n = 11$; CoIC, $n = 6$), or 50 Hz (right; LL, $n = 8$; CoIC, $n = 7$).

Table 4. Differences of short-term plasticity in two pathway (LL vs. CoIC) between two age groups.

Differences in two pathway (LL vs CoIC) in two age groups						
		Tukey			n	
		10 Hz	20 Hz	50 Hz	LL	CoIC
	EPSC	$p < 0.001$	$p < 0.001$	$p < 0.001$	23-24	21
P9-11	AMPA	$p < 0.001$	$p < 0.001$	$p < 0.001$	8-9	6-7
	NMDA	$p < 0.001$	$p < 0.001$	$p < 0.001$	8	8-9
	EPSC	$p=0.77$	$p=0.54$	$p=0.35$	18-23	21
P15-18	AMPA	$p=0.82$	$p=0.99$	$p=0.99$	10	7
	NMDA	$p < 0.01$	$p < 0.001$	$p=0.065$	8-11	6-7

Table 5. Developmental changes of synaptic plasticity (P9–11 vs. P15–18) in LL or CoIC pathway.

Developmental (P9-11 vs P15-18) in LL or CoIC pathway						
		Tukey			n	
		10 Hz	20 Hz	50 Hz	P9-11	P15-18
	EPSC	$p < 0.001$	$p < 0.001$	$p < 0.001$	23-24	18-23
LL	AMPA	$p < 0.01$	$p < 0.001$	$p < 0.001$	8-9	10
	NMDA	$p < 0.001$	$p=0.13$	$p < 0.01$	8	8-11
	EPSC	$p=0.94$	$p=0.09$	$p=0.34$	21	21
CoIC	AMPA	$p=0.99$	$p=0.99$	$p=0.99$	6-7	7
	NMDA	$p=0.99$	$p=0.37$	$p=0.72$	8-9	6-7

Table 6. Differences in the time courses of ANPA and NMDA EPSCs in each pathway.

Differences in the time course of AMPA and NMDA EPSCs						
		Tukey			n	
		10 Hz	20 Hz	50 Hz	AMPA	NMDA
P9-11	LL	$p=0.99$	$p < 0.05$	$p < 0.05$	8-9	8
	CoIC	$p=0.54$	$p < 0.01$	$p=0.23$	6-7	8-9
P15-18	LL	$p=0.99$	$p=0.99$	$p=0.99$	10	8-11
	CoIC	$p=0.77$	$p=0.36$	$p=0.85$	7	6-7

4. Discussion

Developmental changes in the synaptic properties at the CNIC, particularly before and after the onset of hearing, have not been examined quantitatively. This study describes synaptic transmission in the CNIC of P9-11 and P15-18 rats using whole-cell patch clamp recordings from single CNIC neurons. First, I observed accelerated decay of the NMDA-EPSCs in the absence of robust changes in peak amplitudes, whereas the AMPA-EPSCs showed no major changes in the decay kinetics after the onset of hearing. In addition, I found developmental changes in the short-term plasticity elicited by repetitive stimulation of the LL and CoIC pathways. The LL pathway exhibited depression, whereas the CoIC pathway exhibited constant responses or even facilitation at P9-11. This difference between the two pathways was reduced after the onset of hearing (P15-18), when both pathways exhibited slight synaptic depression or facilitation.

4.1. Developmental changes in the EPSC kinetics.

Our data reveal faster decay of the NMDA-EPSCs, after the onset of hearing. The faster decay of NMDA-EPSCs suggests there is an age-dependent switch. Switching of NMDA receptor channels containing (for example) NR2B subunits to those containing NR2A subunits, happen at the calyx of Held (Taschenberger & von Gersdorff, 2000; Futai *et al.*, 2001; Steinert *et al.*, 2010). Alternatively, receptor distribution may change during development, accounting for this difference. This receptor switching hypothesis may be tested in the future using immunostaining, and quantitative measurements of mRNA and protein levels.

In a previous study at the CNIC (Ma *et al.*, 2002), the average NMDA/AMPA ratio decreased up to the time of hearing onset, but not after. I did not find a decline in NMDA/AMPA ratio after hearing onset, either. Some down-regulation of NMDA receptors may happen before hearing onset. In studies of adult rats and bats, NMDARs played multiple roles in signal processing in CNIC adult neurons, and mediated onset responses as well as slow, sustained responses (Zhang & Kelly, 2001; Sanchez *et al.*, 2007). This also suggests that NMDA receptors persist after the onset of hearing. Furthermore, immunostaining suggests that the expression of NMDARs does not change during development (Caicedo & Eybalin, 1999). In other auditory pathways such as the cochlear nucleus and the calyx of Held (Taschenberger & von Gersdorff, 2000; Brenowitz & Trussell, 2001; Iwasaki & Takahashi, 2001; Joshi & Wang, 2002; Taschenberger *et al.*, 2002; Lu & Trussell, 2007), the NMDA-EPSCs are strongly reduced in amplitude during postnatal development at the time of hearing onset. Contrary to this, our data suggest that downregulation of NMDAR expression (as reflected in amplitudes or NMDA/AMPA ratios) does not occur around these 2 weeks of the postnatal period in the CNIC of rats. Because NMDA receptors are important for long-term plasticity (Malenka & Nicoll, 1993), the presence of NMDA receptors may suggest that plasticity may persist after the onset of hearing.

In contrast to NMDA receptors, the decay of AMPA-EPSCs did not change during development. AMPA receptors compose of assemblies of subunits GluR1–4 (or GluR-A–D), each of which has two distinct forms, flip and flop splice variants. In the flop variant, channels are deactivated more rapidly and are desensitized with a faster rate compared with the flip variant (Koike *et al.*, 2000) . Relatively slow decay is consistent with the expression of a GluR-B flip occurring in the IC (Schmid *et al.*,

2001). In the cochlear nucleus and auditory brainstem, the deactivation time course becomes faster with development, and involves switching of receptor subtypes (Geiger *et al.*, 1995; Taschenberger & von Gersdorff, 2000; Iwasaki & Takahashi, 2001; Joshi & Wang, 2002; Lu & Trussell, 2007). Because the MNTB neurons and the cochlear nucleus neurons can phase-lock to kHz sinusoidal amplitude-modulated tones (Grothe, 2000), fast AMPA decay is required for high-frequency signaling in these neurons. In contrast, the IC neurons can phase-lock to a lower frequency (< 100 Hz, Tan et al., 2007) and therefore, AMPA receptor subtype switching may not be required.

4.2. Short-term plasticity of EPSCs before the onset of hearing.

Previous studies have reported that LL-evoked EPSCs showed depression in rats (Wu *et al.*, 2004). Our study in immature rats showed depression, consistent with Wu et al. (2004). In gerbils, EPSCs show facilitation (Vale & Sanes, 2002), which may be most likely due to different species. The AMPA- and NMDA-EPSCs are expected to be reduced in parallel when presynaptic factors such as reduction in presynaptic Ca influx and depletion of the releasable vesicles are involved in synaptic depression (Perkel & Nicoll, 1993; Tong & Jahr, 1994; von Gersdorff *et al.*, 1997). In addition to presynaptic factors, postsynaptic factors such as desensitization of postsynaptic AMPA-EPSCs can be responsible for depression (Trussell *et al.*, 1993; Otis *et al.*, 1996; Koike-Tani *et al.*, 2008). In this study, NMDA-EPSCs had some tendency to show less depression compared to AMPA EPSCs at some frequencies. NMDA receptors are known to exhibit less desensitization and have a higher affinity for glutamate leading to saturation (Perkel & Nicoll, 1993; Tong & Jahr, 1994; von Gersdorff *et al.*, 1997), and these factors together with AMPA receptor desensitization may contribute to synaptic depression

at least to some extent. On the other hand, presynaptic factors augment facilitation and depression at higher frequencies (Zucker & Regehr, 2002), which counteract with postsynaptic factors and cause a complex relationship between the depression (facilitation) time course of AMPA- and NMDA EPSCs.

I have also shown that the CoIC-pathway was facilitated before the onset of hearing. Previous studies in gerbils have shown strong facilitation in immature gerbils (Vale & Sanes, 2002). Facilitation has been shown to be largely mediated by presynaptic mechanisms (Zucker & Regehr, 2002), which could likely explain the facilitation I observed.

Wu et al. (2004) observed a large boost of synaptic responses under voltage clamp, mainly mediated by NMDA receptors, under the influence of inhibitory synaptic currents. They raised the possibility that membrane depolarization occurs at dendrites distant from the recording site, despite the voltage clamp being held at the soma. I might have had similar boosting responses, though I included sufficient concentration of a Na channel blocker QX-314 (5 mM) in most recording conditions for avoiding at least escaped Na currents. Nevertheless, NMDA responses are likely to boost postsynaptic responses under physiological (current clamp) conditions.

4.3. Developmental changes in short-term synaptic plasticity.

The most notable point of this study is that short-term synaptic plasticity changed after the onset of hearing. Although developmental changes of intrinsic connectivity within IC has been examined in detail (Sturm *et al.*, 2014), the changes of afferent synaptic inputs have not been examined previously. I suggest that the occurrence of strong synaptic depression of the LL pathway (Wu et al., 2004) is limited to immature animals. Less pronounced depression observed at the LL

pathway in 2 week old rats is consistent with activity in lower auditory stations, such as the cochlear

nucleus (Brenowitz & Trussell, 2001) and the calyx of Held (Iwasaki et al., 2000; Taschenberger &

von Gersdorff, 2000). Because the AMPA and NMDA EPSCs show a similar time course of

depression after the onset of hearing, presynaptic mechanisms may be mainly responsible for short-

term plasticity (Perkel & Nicoll, 1993; Tong & Jahr, 1994; von Gersdorff et al., 1997). If so,

mechanisms such as reduced release probability and increased synaptic vesicle pool size may be

responsible for developmental changes in the LL pathway, similar to what occurs in the calyx of Held

(Taschenberger & von Gersdorff, 2000; Taschenberger et al., 2002). In addition to the increased

steady-state level, I should note that the steady state is somewhat independent of stimulation

frequency, at least between 10-50 Hz (Weis et al., 1999). Such constant responses assist reliable

transmission from pre- to postsynaptic cells, and this may explain why IC neurons become responsive

to sound reliably at P15 (Shnerson & Willott, 1979). However, I cannot exclude other mechanisms

such as reduced inhibition during development. In contrast to the LL pathway, short-term plasticity

was relatively unchanged in the CoIC pathway. Consequently, both the LL- and CoIC- evoked EPSCs

(especially AMPA-EPSCs) are more balanced, and exhibit similar properties of synaptic responses

and short-term plasticity after the onset of hearing. Such a synaptic arrangement is similar to that

underlying coincidence detection in the auditory brainstem (Cook et al., 2003; Koch & Grothe, 2003;

Kuba et al., 2003; Couchman et al., 2010), where integration is optimized by matching short-term

plasticity of different inputs. In this context, this study may invoke a similar mechanism of excitatory

signal integration from the LL- and CoIC pathways at CNIC neurons. It has been recently shown that

commissural inputs in the IC enhance sound localization in vivo (Orton et al., 2016), and present

findings may have some functional relevance in the context of sound localization.

4.4. Conclusions

The decay of NMDA-EPSCs, but not that of AMPA-EPSCs, was accelerated after the onset of

hearing, facilitating faster responses. However, in contrast to the auditory brainstem, the amplitudes

of NMDA-EPSCs were not reduced. In addition, the present study showed that short-term synaptic

plasticity at excitatory synapses was different in the LL and CoIC pathways at P9–11 but became

similar after hearing onset (Fig. 16). In other words, the data suggest that the relative balance between

LL and CoIC pathways changes depending on the stimulation frequency before hearing onset but

both pathways are more balanced after hearing onset. The sizes of the arrows indicate the relative

synaptic strengths (Fig. 17). Nevertheless, extensive developmental changes occur at synapses that

provide input to the CNIC around the time of hearing onset, with some similarities to those that occur

at auditory relay synapses in the brainstem.
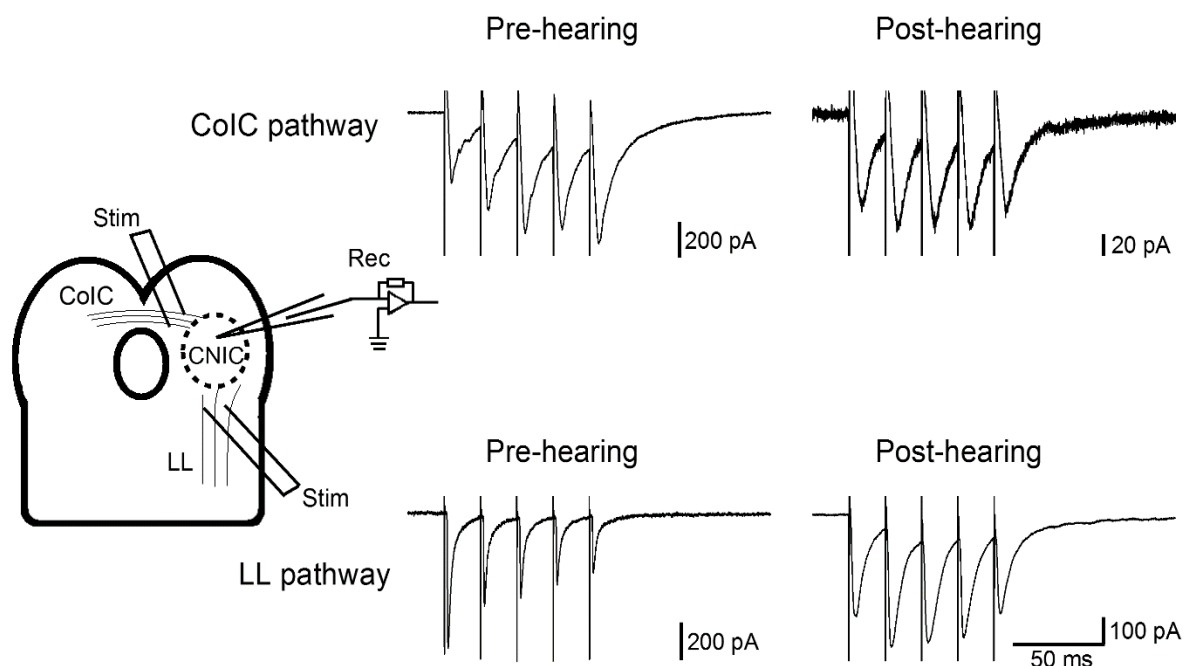
Figure 16. Developmental changes occur at the synapses that input to the CNIC around the time of hearing onset.

49
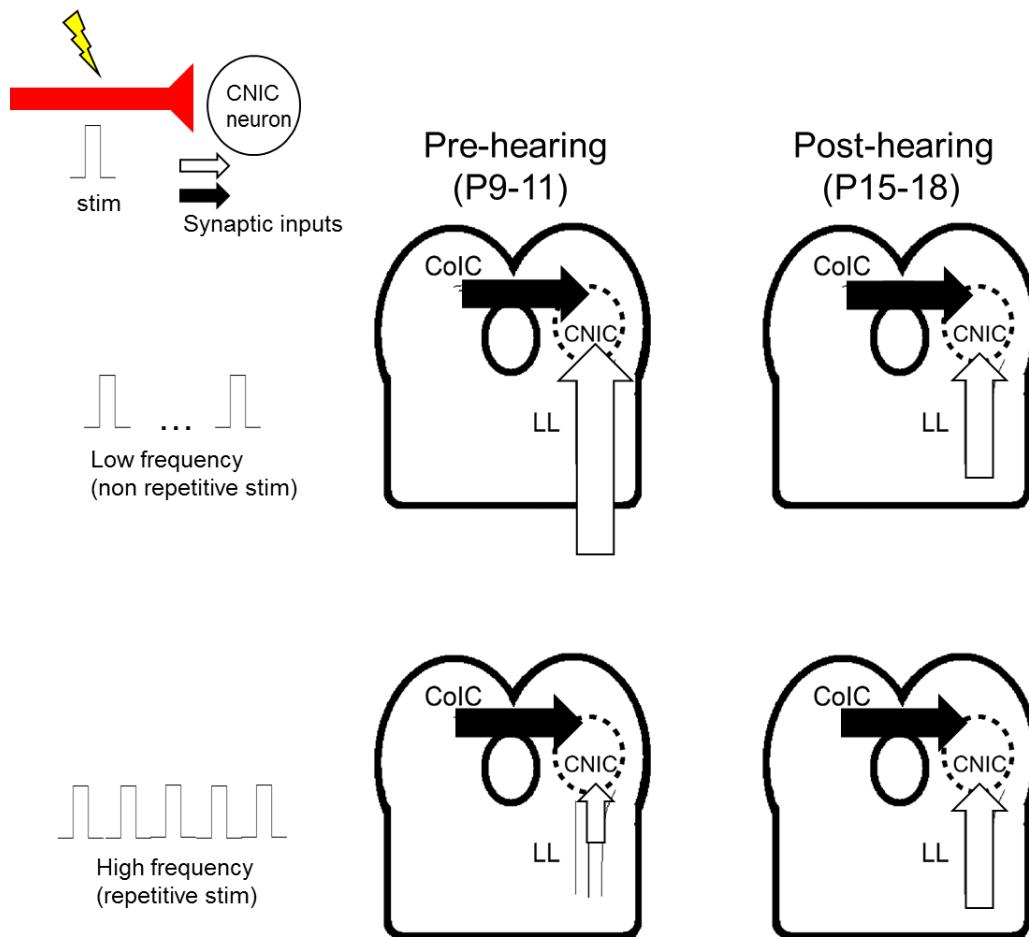
Figure 17. The schematic drawing of changes in synaptic strengths from LL- and CoIC-pathway around onset of hearing.

Strong synaptic depression suggests high release probability of transmitter release and hence high synaptic outputs during low-frequency stimulation, but synaptic strengths are reduced during high-frequency stimulation. This means that a relative balance between LL- and CoIC pathways is changed depending on the stimulation frequency before hearing onset, but both pathways are more balanced irrespective of stimulus frequency after the hearing onset. Sizes of the arrows indicate relative synaptic strengths.

5. Future outlook & concluding remarks

In this study, the excitatory synaptic inputs to the CNIC were analyzed. Before hearing onset, the lemniscus inputs to the IC exhibited short-term depression, whereas commissural inputs showed facilitation. After hearing onset, the EPSCs showed more constant responses during repetitive stimulation in both pathways. These developmental changes ensure a faster and more reliable signal transmission to the CNIC after hearing onset.

5.1. Future outlook

Although I have characterized the basic properties of the excitatory synaptic inputs to the CNIC, several issues remain to be studied.

(1) I have stimulated all ascending synapses together with electrical stimulation. However, the properties may differ between the inputs from different nuclei such as the DCN, MSO, and LSO. This issue can be studied in the future by using selective stimulation of specific nerve fibers using optogenetic stimulation.

(2) Because I found no obvious differences, the data from different types of neurons were pooled together. However, synaptic properties may be different among different cell types, which can be revealed by more detailed studies. For example, large GABAergic neurons in the CNIC have a higher density of glutamatergic synapses on the soma compared to other CNIC neurons (Ito *et al.*, 2009). Such large GABAergic neurons may have different synaptic efficacies.

(3) I saw relatively little developmental changes of the CoIC synapses around the onset of hearing but it remains possible that developmental refinement of the CoIC synapse happens later than

postnatal week two.

(4) What is the cellular mechanism of different forms short-term plasticity between CoIC and LL pathways before the onset of hearing? In addition, is this difference related to a different timing of synaptic formation?

(5) Does presynaptic modulation through mGluRs differ between developmental stages and pathways?

In particular, I should emphasize that the diverse anatomical and physiological features are very challenging for the identification of CNIC neuron types. Recently, Goyer *et al.* (2019) found a specific type of glutamatergic CNIC neurons by using mouse genetics and optogenetics. They found that this cell type receives contralateral DCN and contralateral IC projections. Moreover, they found that the inputs from the DCN activate only AMPA receptors while the CoIC inputs activate both AMPA and NMDA receptors. Such combination of anatomy, physiology, and genetics may allow the dissection of complex IC circuits. It is important to note that they have recorded from mice after P21, but not at postnatal week two like in the present study. Future studies may reveal that NMDA receptors located on CNIC neuron somata may be downregulated much later than the onset of hearing. Nakamoto *et al.* (2013) found that the neurons in the auditory cortex send axonal fibers to the ipsilateral commissural cells in the IC, which in turn send fibers to the contralateral IC (Nakamoto *et al.*, 2013). The CoIC pathway may reflect feedback from the cortex. Future studies will reveal the functional relevance of commissural inputs.

5.2. Concluding remarks

This study revealed developmental changes in synaptic properties at excitatory synapses in the CNIC. Some changes are similar to the auditory brainstem, whereas others are different. In particular, NMDA-EPSCs persist after hearing onset, which may indicate that the synapses are not necessarily adapted to fast auditory signaling. The existence of NMDA receptors may allow room for induction of Hebbian-type synaptic plasticity for which NMDA receptors play a central role (Kandel, et al., 2000). Nevertheless, after the onset of hearing, more reliable synaptic transmission during repetitive stimulation may help for the adaptation of CNIC circuits to more reliable auditory transmission.

6. References

Asaba, A., Hattori, T., Mogi, K., & Kikusui, T. (2014) Sexual attractiveness of male chemicals and vocalizations in mice. *Front. Neurosci.*, **8**, 1–13.

Brenowitz, S. & Trussell, L.O. (2001) Maturation of synaptic transmission at end-bulb synapses of the cochlear nucleus. *J. Neurosci.*, **21**, 9487–9498.

Brian, M. (2013) The nature of sound and the structure and function of the auditory system. In *An Introduction to the Psychology of Hearing*, sixth edit. edn. Brill Academic Publishers, 1–55.

Brunso-Bechtold, J. & Henkel, C. (2005) Development of Auditory Afferents to the Central Nucleus of the Inferior Colliculus. In: Winer J.A., Schreiner C.E. (eds) *The Inferior Colliculus*, Springer, New York, NY, 537–558.

Caicedo, A. & Eybalin, M. (1999) Glutamate receptor phenotypes in the auditory brainstem and mid-brain of the developing rat. *Eur. J. Neurosci.*, **11**, 51–74.

Cant, N.B. (2013) Patterns of convergence in the central nucleus of the inferior colliculus of the mongolian gerbil: organization of inputs from the superior olivary complex in the low frequency representation. *Front. Neural Circuits*, **7**, 1–22.

Cant, N.B. & Benson, C.G. (2006) Organization of the inferior colliculus of the gerbil (meriones unguiculatus): differences in distribution of projections from the cochlear nuclei and the superior olivary complex. *J. Comp. Neurol.*, **495**, 511–528.

Cant, N.B. & Benson, C.G. (2008) Organization of the inferior colliculus of the gerbil (Meriones unguiculatus): Projections from the cochlear nucleus. *Neuroscience*, **154**, 206–217.

Caspary, D.M., Ling, L., Turner, J.G., & Hughes, L.F. (2008) Inhibitory neurotransmission , plasticity and aging in the mammalian central auditory system. *J. Exp. Biol.*, **211**, 1781–1791.

Clause, A., Kim, G., Sonntag, M., Weisz, C.J.C., Vetter, D.E., Rubsamen, R., & Kandler, K. (2014) The Precise Temporal Pattern of Prehearing Spontaneous Activity Is Necessary for Tonotopic Map Refinement. *Neuron*, **82**, 822–835.

Clopton, B.M. & Winfield, J.A. (1976) Effect of early exposure to patterned sound on unit activity in rat inferior colliculus. *J. Neurophysiol.*, **39**, 1081–1089.

Cook, D.L., Schwindt, P.C., Grande, L.A., & Spain, W.J. (2003) Synaptic depression in the localization of sound. *Nature*, **421**, 66–70.

Couchman, K., Grothe, B., & Felmy, F. (2010) Medial superior olivary neurons receive surprisingly few excitatory and inhibitory inputs with balanced strength and short-term dynamics. *J. Neurosci.*, **30**, 17111–17121.

Crins, T.T.H., Rusu, S.I., Rodriguez-Contreras, A., & Borst, J.G.G. (2011) Developmental changes in short-term plasticity at the rat calyx of Held synapse. *J. Neurosci.*, **31**, 11706–11717.

del Castillo, J. & Katz, B. (1954) Quantal components of the end‑plate potential. *J. Physiol.*, **124**, 560–573.

Ehret, G. & Schreiner, C. (2005) Spectral and Intensity Coding in the Auditory Midbrain. In: Winer J.A., Schreiner C.E. (eds) *The Inferior Colliculus*, Springer, New York, NY, 312–345.

Erazo-Fischer, E., Striessnig, J., & Taschenberger, H. (2007) The role of physiological afferent nerve activity during in vivo maturation of the calyx of Held synapse. *J. Neurosci.* **27**, 1725-

37.

Friauf, E., Fischer, A.U., & Fuhr, M.F. (2015) Synaptic plasticity in the auditory system: a review. *Cell Tissue Res.*, **361**, 177–213.

Futai, K., Okada, M., Matsuyama, K., & Takahashi, T. (2001) High-fidelity transmission acquired via a developmental decrease in NMDA receptor expression at an auditory synapse. *J. Neurosci.*, **21**, 3342–3349.

Gabriele, M.L., Brunso-Bechtold, J.K., & Henkel, C.K. (2000) Development of afferent patterns in the inferior colliculus of the rat: Projection from the dorsal nucleus of the lateral lemniscus. *J. Comp. Neurol.*, **416**, 368–382.

Geiger, J.R.P., Melcher, T., Koh, D.S., Sakmann, B., Seeburg, P.H., Jonas, P., & Monyer, H. (1995) Relative abundance of subunit mRNAs determines gating and Ca2+ permeability of AMPA receptors in principal neurons and interneurons in rat CNS. *Neuron*, **15**, 193–204.

Glasgow, N.G., Siegler Retchless, B., & Johnson, J.W. (2015) Molecular bases of NMDA receptor subtype-dependent properties. *J. Physiol.*, **593**, 83–95.

Grécová, J., Bureš, Z., Popelář, J., Šuta, D., & Syka, J. (2009) Brief exposure of juvenile rats to noise impairs the development of the response properties of inferior colliculus neurons. *Eur. J. Neurosci.*, **29**, 1921–1930.

Grothe, B. (2000) The evolution of temporal processing in the medial superior olive, an auditory brainstem structure. *Prog. Neurobiol.*, **61**, 581–610.

Iacobucci, G.J. & Popescu, G.K. (2017) NMDA receptors : linking physiological output to biophysical operation. *Nat. Rev. Neurosci.*, **18**, 236–249.

Ito, T., Bishop, D.C., & Oliver, D.L. (2009) Two Classes of GABAergic Neurons in the Inferior Colliculus. *J. Neurosci.*, **29**, 13860–13869.

Ito, T. & Malmierca, M. (2018) Neurons, Connections, and Microcircuits of the Inferior Colliculus. In: Oliver D., Cant N., Fay R., Popper A. (eds) *The Mammalian Auditory Pathways*, Springer Handbook of Auditory Research, **65**, Springer, Cham, 127–167.

Ito, T. & Oliver, D.L. (2014) Local and commissural IC neurons make axosomatic inputs on large GABAergic tectothalamic neurons. *J. Comp. Neurol.*, **522**, 3539–3554.

Iwasaki, S. & Takahashi, T. (2001) Developmental regulation of transmitter release at the calyx of Held in rat auditory brainstem. *J. Physiol.*, **534**, 861–871.

Joshi, I. & Wang, L. (2002) Developmental profiles of glutamate receptors and synaptic transmission at a single synapse in the mouse auditory brainstem. *J. Physiol.*, **540**, 861–873.

Kandel, E.R., Schwartz, J.H., Jessell, T.M., Jessell, D. of B. and M.B.T., Siegelbaum, S., & Hudspeth, A.J. (2000) *Principles of Neural Science*. McGraw-hill New York.

Kasai, M., Ono, M., & Ohmori, H. (2012) Distinct neural firing mechanisms to tonal stimuli offset in the inferior colliculus of mice in vivo. *Neurosci. Res.*, **73**, 224–237.

Kelly J.B. & Caspary D.M. (2005) Pharmacology of the Inferior Colliculus. In: Winer J.A., Schreiner C.E. (eds) *The Inferior Colliculus,* Springer, New York, NY, pp. 248–281.

Kim, G. & Kandler, K. (2010) Synaptic changes underlying the strengthening of GABA/glycinergic connections in the developing lateral superior olive. *Neuroscience*, **171**, 924–933.

Kitagawa, M. & Sakaba, T. (2019) Developmental changes in the excitatory short-term plasticity at input synapses in the rat inferior colliculus. *Eur. J. Neurosci.*, **50**, 2830–2846.

Knudsen, E.I. (2002) Instructed learning in the auditory localization pathway of the barn owl.

Nature, **417**, 322–328.

Koch, U. & Grothe, B. (2003) Hyperpolarization-activated current (Ih) in the inferior colliculus: distribution and contribution to temporal processing. *J. Neurophysiol.*, **90**, 3679–3687.

Koike-Tani, M., Kanda, T., Saitoh, N., Yamashita, T., & Takahashi, T. (2008) Involvement of AMPA receptor desensitization in short-term synaptic depression at the calyx of Held in developing rats. *J. Physiol.*, **586**, 2263–2275.

Koike, M., Tsukada, S., Tsuzuki, K., Kijima, H., & Ozawa, S. (2000) Regulation of kinetic properties of GluR2 AMPA receptor channels by alternative splicing. *J. Neurosci.*, **20**, 2166–2174.

Kuba, H., Yamada, R., & Ohmori, H. (2003) Evaluation of the limiting acuity of coincidence detection in nucleus laminaris of the chicken. *J. Physiol.*, **552**, 611–620.

Lu, T. & Trussell, L.O. (2007) Development and elimination of endbulb synapses in the chick cochlear nucleus. *J. Neurosci.*, **27**, 808–817.

Ma, C.L., Kelly, J.B., & Wu, S.H. (2002) AMPA and NMDA receptors mediate synaptic excitation in the rat's inferior colliculus. *Hear. Res.*, **168**, 25–34.

Magnusson, A.K., Kapfer, C., Grothe, B., & Koch, U. (2005) Maturation of glycinergic inhibition in the gerbil medial superior olive after hearing onset. *J. Physiol.*, **568**, 497–512.

Malenka, R.C. & Nicoll, R.A. (1993) NMDA-receptor-dependent synaptic plasticity: multiple forms and mechanisms. *Trends Neurosci.*, **16**, 521–527.

Malmierca, M.S., Hernández, O., Antunes, F.M., & Rees, A. (2009) Divergent and point-to-point connections in the commissural pathway between the inferior colliculi. *J. Comp. Neurol.*, **514**, 226–239.

Malmierca, M.S., Hernández, O., & Rees, A. (2005) Intercollicular commissural projections modulate neuronal responses in the inferior colliculus. *Eur. J. Neurosci.*, **21**, 2701–2710.

Moore, D.R., Kotak, V.C., & Sanes, D.H. (1998) Commissural and lemniscal synaptic input to the gerbil inferior colliculus. *J. Neurophysiol.*, **80**, 2229–2236.

Moore, L.A. & Trussell, L.O. (2017) Corelease of Inhibitory Neurotransmitters in the Mouse Auditory Midbrain. *J. Neurosci.*, **37**, 9453–9464.

Nakamoto, K.T., Sowick, C.S., & Schofield, B.R. (2013) Auditory cortical axons contact commissural cells throughout the guinea pig inferior colliculus. *Hear. Res.*, **306**, 131–144.

Neher, E. (2017) Some Subtle Lessons from the Calyx of Held Synapse. *Biophys. J.*, **112**, 215–223.

Oliver, D.L. (2005) Neuronal organization in the inferior colliculus. In: Winer J.A., Schreiner C.E. (eds) *The Inferior Colliculus*, Springer, New York, NY, 69–114.

Ono, M., Bishop, D.C., & Oliver, D.L. (2017) Identified GABAergic and glutamatergic neurons in the mouse inferior colliculus share similar response properties. *J. Neurosci.*, **37**, 8952–8964.

Ono, M. & Ito, T. (2015) Functional organization of the mammalian auditory midbrain. *J. Physiol. Sci.*, **65**, 499–506.

Ono, M. & Oliver, D.L. (2014) The balance of excitatory and inhibitory synaptic inputs for coding sound location. *J. Neurosci.*, **34**, 3779–3792.

Ono, M., Yanagawa, Y., & Koyano, K. (2005) GABAergic neurons in inferior colliculus of the GAD67-GFP knock-in mouse: Electrophysiological and morphological properties. *Neurosci. Res.*, **51**, 475–492.

Orton, L.D., Papasavvas, C.A., & Rees, A. (2016) Commissural gain control enhances the midbrain

representation of sound location. *J. Neurosci.*, **36**, 4470–4481.

Otis, T., Zhang, S., & Trussell, L.O. (1996) Direct measurement of AMPA receptor desensitization induced by glutamatergic synaptic transmission. *J. Neurosci.*, **16**, 7496–7504.

Palmer, A.R., Shackleton, T.M., Sumner, C.J., Zobay, O., & Rees, A. (2013) Classification of frequency response areas in the inferior colliculus reveals continua not discrete classes. *J. Physiol.*, **591**, 4003–4025.

Pérez-González, D. & Malmierca, M.S. (2014) Adaptation in the auditory system: An overview. *Front. Integr. Neurosci.*, **8**, 1–10.

Perkel, D.J. & Nicoll, R.A. (1993) Evidence for all‐or‐none regulation of neurotransmitter release: implications for long‐term potentiation. *J. Physiol.*, **471**, 481–500.

Peruzzi, D., Sivaramakrishnan, S., & Oliver, D.L. (2000) Identification of cell types in brain slices of the inferior colliculus. *Neuroscience*, **101**, 403–416.

Reetz, G. & Ehret, G. (1999) Inputs from three brainstem sources to identified neurons of the mouse inferior colliculus slice. *Brain Res.*, **816**, 527–543.

Regehr, W.G. (2012) Short-term presynaptic plasticity. *Cold Spring Harb. Perspect. Biol.*, **4**, 1–19.

Regehr, W.G. & Abbott, L.F. (2004) Synaptic computation. *Nature*, **431**, 796–803.

Saldaña, E., Aparicio, M.A., Fuentes-Santamaría, V., & Berrebi, A.S. (2009) Connections of the superior paraolivary nucleus of the rat: projections to the inferior colliculus. *Neuroscience*, **163**, 372–387.

Saldaña, E. & Merchań, M.A. (1992) Intrinsic and commissural connections of the rat inferior colliculus. *J. Comp. Neurol.*, **319**, 417–437.

Sanchez, J.T., Gans, D., & Wenstrup, J.J. (2007) Contribution of NMDA and AMPA receptors to temporal patterning of auditory responses in the inferior colliculus. *J. Neurosci.*, **27**, 1954–1963.

Sanchez, J.T., Ghelani, S., & Otto-Meyer, S. (2015) From development to disease: Diverse functions of NMDA-type glutamate receptors in the lower auditory pathway. *Neuroscience*, **285**, 248–259.

Schmid, S., Guthmann, A., & Ruppersberg, J.P. (2001) Expression of AMPA receptor subunit flip/flop splice variants in the rat auditory brainstem and inferior colliculus. *J. Comp. Neurol.*, **430**, 160–171.

Schneggenburger, R. & Forsythe, I.D. (2006) The calyx of Held. *Cell Tissue Res.*, **326**, 311–337.

Shnerson, A. & Willott, J.F. (1979) Development of inferior colliculus response properties in C57BL/6J mouse pups. *Exp. Brain Res.*, **37**, 373–385.

Sivaramakrishnan, S. & Oliver, D.L. (2001) Distinct K currents result in physiologically distinct cell types in the inferior colliculus of the rat. *J. Neurosci.*, **21**, 2861–2877.

Sivaramakrishnan, S. & Oliver, D.L. (2006) Neuronal responses to lemniscal stimulation in laminar brain slices of the inferior colliculus. *JARO*, **7**, 1–14.

Steinert, J.R., Postlethwaite, M., Jordan, M.D., Chernova, T., Robinson, S.W., & Forsythe, I.D. (2010) NMDAR-mediated EPSCs are maintained and accelerate in time course during maturation of mouse and rat auditory brainstem in vitro. *J. Physiol.*, **588**, 447–463.

Sturm, J., Nguyen, T., & Kandler, K. (2014) Development of intrinsic connectivity in the central nucleus of the mouse inferior colliculus. *J. Neurosci.*, **34**, 15032–15046.

Taschenberger, H., Leão, R.M., Rowland, K.C., Spirou, G.A., & von Gersdorff, H. (2002)

Optimizing synaptic architecture and efficiency for high-frequency transmission. *Neuron*, **36**, 1127–1143.

Taschenberger, H. & von Gersdorff, H. (2000) Fine-tuning an auditory synapse for speed and fidelity: developmental changes in presynaptic waveform, EPSC kinetics, and synaptic plasticity. *J. Neurosci.*, **20**, 9162–9173.

Tong, G. & Jahr, C.E. (1994) Multivesicular release from excitatory synapses of cultered hippocampal neurons. *Neuron*, **12**, 51–59.

Trussell, L.O., Zhang, S., & Ramant, I.M. (1993) Desensitization of AMPA receptors upon multiquantal neurotransmitter release. *Neuron*, **10**, 1185–1196.

Vale, C., Juíz, J.M., Moore, D.R., & Sanes, D.H. (2004) Unilateral cochlear ablation produces greater loss of inhibition in the contralateral inferior colliculus. *Eur. J. Neurosci.*, **20**, 2133–2140.

Vale, C. & Sanes, D.H. (2002) The effect of bilateral deafness on excitatory and inhibitory synaptic strength in the inferior colliculus. *Eur. J. Neurosci.*, **16**, 2394–2404.

von Gersdorff, H. & Borst, J.G.G. (2002) Short-term plasticity at the calyx of held. *Nat. Rev. Neurosci.*, **3**, 53–64.

von Gersdorff, H., Schneggenburger, R., Weis, S., & Neher, E. (1997) Presynaptic depression at a calyx synapse: the small contribution of metabotropic glutamate receptors. *J. Neurosci.*, **17**, 8137–8146.

Wang, H.C. & Bergles, D.E. (2015) Spontaneous activity in the developing auditory system. *Cell Tissue Res.*, **361**, 65–75.

Weis, S., Schneggenburger, R., & Neher, E. (1999) Properties of a model of Ca++-dependent vesicle pool dynamics and short term synaptic depression. *Biophys. J.*, **77**, 2418–2429.

Winer, J.A. & Schreiner, C.E. (2005) The Central Auditory System: A Functional Analysis. In: Winer J.A., Schreiner C.E. (eds) *The Inferior Colliculus*, Springer, New York, NY, 1–68.

Wu, S.H., Lei, M.C., & Kelly, J.B. (2004) Contribution of AMPA, NMDA, and GABA(A) receptors to temporal pattern of postsynaptic responses in the inferior colliculus of the rat. *J. Neurosci.*, **24**, 4625–4634.

Yassin, L., Pecka, M., Kajopoulos, J., Gleiss, H., Li, L., Leibold, C., & Felmy, F. (2016) Differences in synaptic and intrinsic properties result in topographic heterogeneity of temporal processing of neurons within the inferior colliculus. *Hear. Res.*, **341**, 79–90.

Zhang, H. & Kelly, J.B. (2001) AMPA and NMDA receptors regulate responses of neurons in the rat's inferior colliculus. *J. Neurophysiol.*, **86**, 871–880.

Zucker, R.S. & Regehr, W.G. (2002) Short-term synaptic plasticity. *Annu. Rev. Physiol.*, **64**, 355–405.